

# CP Violation in the Minimal Linear $\sigma$ Model

**J. Alonso-González<sup>a)\*</sup>, J.M. Lizana<sup>b)†</sup>, V. Martínez-Fernández<sup>c)‡</sup>,  
L. Merlo<sup>a)§</sup>, and S. Pokorski<sup>d)¶</sup>**

<sup>a)</sup> Departamento de Física Teórica and Instituto de Física Teórica UAM/CSIC,  
Universidad Autónoma de Madrid, Cantoblanco, 28049, Madrid, Spain

<sup>b)</sup> Physik-Institut, Universität Zürich, CH-8057 Zürich, Switzerland

<sup>c)</sup> National Centre for Nuclear Research (NCBJ),  
Pasteura 7, 02-093 Warsaw, Poland

<sup>d)</sup> Institute of Theoretical Physics, Faculty of Physics,  
University of Warsaw, Pasteura 5, PL 02-093, Warsaw, Poland

## Abstract

Beyond the Standard Model frameworks usually present new CP violating sources generically leading to pseudoscalar components in the effective Standard Model Yukawa couplings. They are strongly bounded by the electric dipole moments, particularly for the top quark Yukawa, but can be large enough for successful electroweak baryogenesis when all third generation fermions are considered. Additional necessary condition is that the electroweak phase transition is strong enough. However, strong bounds on the top Yukawa coupling raise the question how natural is its very small pseudoscalar component if not suppressed by a very large new physics scale. In this paper, all those issues are discussed in the framework of the Minimal Linear  $\sigma$  Model with CP violating phases, that represent the only example of renormalisable model embedding the Minimal Composite Higgs model.

---

\*[j.alonso.gonzalez@csic.es](mailto:j.alonso.gonzalez@csic.es);  [orcid.org/0000-0002-0345-3860](https://orcid.org/0000-0002-0345-3860)

†[jlizana@physik.uzh.ch](mailto:jlizana@physik.uzh.ch);  [orcid.org/0000-0002-2998-7158](https://orcid.org/0000-0002-2998-7158)

‡[Victor.Martinez-fernandez@ncbj.gov.pl](mailto:Victor.Martinez-fernandez@ncbj.gov.pl);  [orcid.org/0000-0002-0581-7154](https://orcid.org/0000-0002-0581-7154)

§[luca.merlo@uam.es](mailto:luca.merlo@uam.es);  [orcid.org/0000-0002-5876-4105](https://orcid.org/0000-0002-5876-4105)

¶[Stefan.Pokorski@fuw.edu.pl](mailto:Stefan.Pokorski@fuw.edu.pl);  [orcid.org/0000-0002-3750-1330](https://orcid.org/0000-0002-3750-1330)

# Contents

<b>1</b>	<b>Introduction</b>	<b>1</b>
<b>2</b>	<b>The Minimal Linear <math>\sigma</math> Model</b>	<b>3</b>
2.1	The Scalar Sector . . . . .	4
2.2	The Fermionic Sector . . . . .	7
2.3	The Low-Energy Effective Operators . . . . .	11
<b>3</b>	<b>The Electric Dipole Moment</b>	<b>13</b>
3.1	Numerical Results . . . . .	15
<b>4</b>	<b>Electroweak Phase Transition</b>	<b>18</b>
4.1	Leading Temperature Corrections . . . . .	19
4.2	Full Analysis . . . . .	21
<b>5</b>	<b>Conclusions</b>	<b>22</b>
<b>A</b>	<b>Finite Temperature Effective Potential</b>	<b>23</b>
A.1	High Temperature Approximation . . . . .	25

## 1 Introduction

The CP violation in the Standard Model (SM) is controlled by the CKM matrix. In extensions of the SM there are, generically, new potential sources of CP violation (CPV). This is interesting since CP sensitive observables can provide probes of new physics (NP) and, moreover, beyond the SM sources of CPV are needed for the electroweak baryogenesis.

One of the best CP sensitive observables are electric dipole moments (EDMs). The SM predictions for the fermion EDMs give extremely small values and therefore any NP contribution associated to new sources of CPV may show up at experiments as a clear signal of Beyond the SM (BSM) physics. On the other hand, present experimental bounds on fermion EDMs provide extremely strong bounds on BSM scenarios, such as supersymmetry or composite Higgs (CH) models, or more in general as flavour models.

In particular the electron EDM is at present the one with strongest bounds. The SM prediction turns out to be accidentally highly suppressed,  $\approx 10^{-44}$  e cm [1], while the present bound from the ACME II collaboration [2] is

$$|d_e| < 1.1 \times 10^{-29} \text{ e cm} \quad \text{at 90\% C.L.}, \quad (1.1)$$

where  $d_e$  is defined in the following effective Lagrangian

$$\mathcal{L}_{\text{EDM}} = -\frac{i d_e}{2} \bar{e} \sigma_{\mu\nu} \gamma_5 e F^{\mu\nu} \quad \text{with} \quad \sigma_{\mu\nu} \equiv \frac{i}{2} [\gamma_\mu \gamma_\nu - \gamma_\nu \gamma_\mu]. \quad (1.2)$$

The constraint in Eq. (1.1) may infer a lower bound on NP scale that is even higher than the energies presently studied at colliders [3–5].

The aim of the present paper is to study the effects of CPV sources in a specific model of composite Higgs with a particular emphasis in the electron EDM. The framework under consideration is the so-called Minimal Linear  $\sigma$  Model (ML $\sigma$ M) [6] that is a renormalisable model that attempts to improve the limitation of the traditional CH models [7–15]. In the latter, the indetermination of the strong dynamics, responsible for the breaking of the initial global symmetry, leads to the effective Lagrangian that has a limited range of application. On the contrary, the ML $\sigma$ M is renormalisable and therefore any quantity is completely computable.

The ML $\sigma$ M is based on the global spontaneous symmetry breaking  $SO(5) \rightarrow SO(4)$  and matches the minimal CH model [13, 16, 17] in a specific limit. It is constructed introducing a scalar quintuplet of  $SO(5)$  that contains the three SM Goldstone Bosons (GBs), the Higgs and an additional electroweak (EW) singlet  $\sigma$ . The spectrum is also enlarged by the addition of several exotic fermions in the trivial and fundamental representations of  $SO(5)$  that play a role in the fermion partial compositeness mechanism [12, 18, 19]. One of the novelties of the ML $\sigma$ M with respect the traditional CH models resides in the fact that the whole spectrum of the exotic fermions and their interactions are fixed in terms of the initial Lagrangian parameters.

The ML $\sigma$ M has already been highly investigated: its low-energy features have been studied in Ref. [20], projecting to the so-called Higgs Effective Field Theory Lagrangian [21–34]; the possibility to solve the strong CP problem within the ML $\sigma$ M has been analysed in Refs. [35–37]; the phenomenology associated to the lightest exotic fermions has been illustrated in Ref. [38].

The main goal of this paper is to generalise the ML $\sigma$ M Lagrangian, which was taken to be strictly CP conserving, to have arbitrary complex Lagrangian parameters, that is to have additional sources of CP violation. The electron EDM will receive NP contributions due to the modifications of the Higgs couplings to the third generation fermions, after integrating out the heavy degrees of freedom (dofs). The effective Lagrangian describing the fermion-Higgs couplings can be parametrised as

$$\mathcal{L}_{\text{eff}} \supset -\frac{y_\psi}{\sqrt{2}} (\kappa_\psi \bar{\psi} \psi + i \tilde{\kappa}_\psi \bar{\psi} \gamma_5 \psi) h \quad \text{with} \quad y_\psi \equiv \frac{\sqrt{2} m_\psi}{v_h}, \quad (1.3)$$

where  $v_h = 246$  GeV is the EW symmetry breaking vacuum expectation value (VEV) of the Higgs field,  $m_\psi$  the mass of the  $\psi$  fermion. Ref. [39] has studied in details the impact of generic modifications of the third family fermion couplings with the Higgs in the electron EDM and their analysis will be taken as a reference for the computational part of this paper.

The electron EDM puts a constraint on the three-dimensional space of the effective fermion parameters  $\tilde{\kappa}_t, \tilde{\kappa}_b, \tilde{\kappa}_\tau$ , with upper bounds on each of them (for a recent analysis see Ref. [40]). Particularly strong bounds are obtained for  $\tilde{\kappa}_t, \tilde{\kappa}_\tau < \mathcal{O}(10^{-3})$ . In general, the NP is expected to modify all Yukawa couplings, so the focus in this paper will be on the most constrained top coupling. In extensions of the SM based on the EFT approach, the SM Lagrangian is supplemented by higher dimension operators suppressed by effective scale  $\Lambda$ , with arbitrary Wilson coefficients. In SMEFT, the leading operators contributing to the effective Yukawa couplings are  $d = 6$ , with the coefficients  $c/\Lambda^2 = |c|e^{i\alpha}/\Lambda^2$ . The

bounds on the  $\tilde{\kappa}_\psi$  can be translated, for generic values of the moduli  $|c_\psi|$ , into the bounds on the new phases as a function of the effective NP scale. For instance, for  $\Lambda \sim \mathcal{O}(1 \text{ TeV})$ , the phase  $\alpha_t$  can be at most  $\mathcal{O}(10^{-2})$ . Of course, the higher the effective scale the larger the phase can be, but one may wonder if a relatively low scales can be compatible with naturalness, unless some explanation for the smallness of the phase is given.

In the UV complete model considered in this paper the effective couplings  $\tilde{\kappa}_\psi$  are calculable in terms of the original Lagrangian parameters. Equivalently, the Wilson coefficients of the dominant, in this model,  $d = 5$  low-energy operators are calculable in terms of the Lagrangian parameters. One might expect that the presence of the  $d = 5$  operators contributing to the effective Yukawa couplings would imply even stronger fine tuning of the phases. Indeed, such a conclusion follows from the parametrisation of the Wilson coefficients in terms of the effective scale  $\Lambda$ ,  $c/\Lambda = |c|e^{i\alpha}/\Lambda$  for  $d = 5$ . However, as shown in the first part of the paper, the intuition based on a single effective scale and single coupling is misleading. The ML $\sigma$ M model is an example that a rich structure of an UV complete model may allow for much more natural values of the phases, even compared with the SMEFT  $d = 6$  operators.

It is well known that the same effective parameters  $\tilde{\kappa}_\psi$  are responsible for the contribution of different third generation fermions to the baryon asymmetry in the universe in the electroweak phase transitions, *provided* it is a strong enough first order transition (see Refs. [40–45]), which is not the case in the SM. In particular, the ML $\sigma$ M can be easily extended to the lepton sector and a complex  $\tau$  Yukawa coupling can account for the observed asymmetry as the EDM bounds on it are much weaker. In the EFT approach, different operators contribute to the Yukawa couplings and to the Higgs potential, so one can disentangle the two questions and that is indeed the often taken path. However, in a UV complete model like the one studied in this paper, such a freedom does not exist. The character of the phase transition depends on the scalar potential and the temperature effects and it is totally predictable. As discussed in Sect. 4, for the parameter range consistent with the present experimental data, it turns out to be by far too weak for a successful electroweak baryogenesis. Thus, the ML $\sigma$ M is an interesting example with potentially large enough new sources of CPV but nevertheless failing for the electroweak baryogenesis.

The structure of the paper can be read out in the table of contents.

## 2 The Minimal Linear $\sigma$ Model

The global symmetry group of the ML $\sigma$ M is  $SO(5) \times U(1)_X$ , where the last Abelian factor ensures the correct hypercharge assignment for the SM fields. The gauge sector coincides with the one of the SM, while the scalar spectrum contains a real scalar field  $\phi$  in the fundamental representation of  $SO(5)$ . The fermionic sector contain elementary fermions with the same quantum numbers as in the SM and exotic vector-like quarks in the trivial and fundamental representation of  $SO(5)$ .

The scalar field  $\phi$  has five components that can be identified with the three would-be-longitudinal components of the SM gauge bosons  $\pi_i$ ,  $i = 1, 2, 3$ , the Higgs field  $\mathbf{h}$  and the

	$\phi$	$\psi^{(2/3)}$	$\chi^{(2/3)}$	$\psi^{(-1/3)}$	$\chi^{(-1/3)}$
$SO(5)$	5	5	1	5	1
$U(1)_X$	0	+2/3	+2/3	-1/3	-1/3

Table 1: Transformation properties of the scalar and exotic fields under  $SO(5) \times U(1)_X$ . The superscripts (2/3) and (-1/3) on the fermionic fields refer to the top and bottom quark sectors.

additional scalar field  $\mathbf{s}$ , singlet under the SM group:

$$\phi = (\pi_1, \pi_2, \pi_3, \mathbf{h}, \mathbf{s})^T \xrightarrow{u.g.} \phi = (0, 0, 0, \mathbf{h}, \mathbf{s})^T, \quad (2.1)$$

where the last expression holds in the unitary gauge and unbroken phase. The scalar potential that can be constructed with this field is then responsible for the spontaneous breaking of  $SO(5)$  down to  $SO(4)$ . Additional explicit breaking terms are added to the scalar potential to drive the  $SO(4)$  and EW symmetry breaking, as discussed in Ref. [6].

The scalar field  $\phi$  only couples directly to the exotic fermions, and in particular does not have direct couplings with the elementary fermions. Therefore neither the SM Higgs couples at tree-level to the elementary fermions. Such couplings arise only through the mediation of the exotic fermions, as for the active neutrinos in the Seesaw mechanisms that acquire masses and couplings with the Higgs only via the mediations of heavy states. The exotic fermions have  $U(1)_X$  charges equal to 2/3 or -1/3 and are associated to the up-type and down-type sectors, respectively. The proto-Yukawas are couplings between the  $SO(5)$  quintuplet VLQs  $\psi$ , the singlets  $\chi$  and the scalar field  $\phi$ . The charged lepton sector can also be described by adding a copy of the down-quark Lagrangian with exotic fermions with  $U(1)_X = -1$ . For shortness, terms including charged leptons will not be shown explicitly and only comments will be added when necessary.

Tab. 1 summarises the scalar and exotic fermion fields appearing in the model with their transformation properties under  $SO(5) \times U(1)_X$ . Notice that the original version of the ML $\sigma$ M only contains one flavour generation: as in the Seesaw mechanism, the heavier is the elementary field the lighter is the exotic sibling responsible of its mass; it follows that the relevant phenomenology associated to the exotic fermion sector reduces to the one associated to the top, bottom and  $\tau$  sectors, while the lighter flavour generations can be assumed to be SM like. The same assumption will be taken in this paper, focussing on the effects of the top, bottom and  $\tau$  partners, assuming that first and second generation elementary fermions have exactly the SM masses and couplings.

## 2.1 The Scalar Sector

The spontaneous breaking of  $SO(5)$  first and of  $SO(4)$  and the EW symmetries later is described by the scalar potential  $V(\phi)$

$$V(\phi) = \lambda (\phi^T \phi - f^2)^2 + \alpha f^3 \mathbf{s} - \beta f^2 \mathbf{h}^2, \quad (2.2)$$

where  $f$  is the scale at which the  $SO(5)$  breaking takes place. The last two terms, proportional to  $\alpha$  and  $\beta$ , as two soft breaking terms that are required in order to absorb the one-loop Coleman-Weinberg contributions (see Ref. [36] for a different treatment). Notice that  $\lambda$  controls the non-linearity of the model: in the  $\lambda \gg 1$  limit, that corresponds to decouple the  $\sigma$  field from the low-energy theory, the  $ML\sigma M$  converges in the minimal CH model.

Once the  $SO(4)$  and EW symmetry breaking takes place, then  $\mathbf{h}$  and  $\mathbf{s}$  develop a VEV:

$$\mathbf{h} = \hat{\mathbf{h}} + v_{\mathbf{h}}, \quad \mathbf{s} = \hat{\mathbf{s}} + v_{\mathbf{s}}, \quad (2.3)$$

where the normalisation has been chosen to match Eq. (2.1). While these two VEVs are undefined if  $\alpha = 0 = \beta$ , their general expression turns out to be

$$v_{\mathbf{s}}^2 = f^2 \frac{\alpha^2}{4\beta^2}, \quad v_{\mathbf{h}}^2 = f^2 \left( 1 - \frac{\alpha^2}{4\beta^2} + \frac{\beta}{2\lambda} \right), \quad (2.4)$$

with

$$v_{\mathbf{h}}^2 + v_{\mathbf{s}}^2 = f^2 \left( 1 + \frac{\beta}{2\lambda} \right). \quad (2.5)$$

A few conditions apply to these parameters. The  $SO(5)$  breaking requires that  $f^2 > 0$ , while imposing that the Higgs arises as a GB leads to  $|v_{\mathbf{h}}| < |v_{\mathbf{s}}|$ : it follows that

$$2\beta^2 \left( 1 + \frac{\beta}{2\lambda} \right) < \alpha^2 < 4\beta^2 \left( 1 + \frac{\beta}{2\lambda} \right) \quad (2.6)$$

which in the  $\alpha, \beta \ll \lambda$  limit reads as

$$2\beta^2 \leq \alpha^2 \leq 4\beta^2. \quad (2.7)$$

If one then imposes that  $v_{\mathbf{h}}^2 \ll f^2$ , then an additional condition follows,

$$-\frac{\alpha^2}{4\beta^2} + \frac{\beta}{2\lambda} \ll 1, \quad (2.8)$$

than further simplifies in the  $\alpha, \beta \ll \lambda$  limit,

$$\alpha/2\beta \sim 1. \quad (2.9)$$

Once the symmetries get broken, a non diagonal  $2 \times 2$  mass matrix can be read out from Eq. (2.2). The mass eigenstates  $h, \sigma$ , after diagonalising this mass matrix, can be defined as

$$h = \hat{\mathbf{h}} \cos \gamma - \hat{\mathbf{s}} \sin \gamma, \quad \sigma = \hat{\mathbf{h}} \sin \gamma + \hat{\mathbf{s}} \cos \gamma, \quad (2.10)$$

where the mixing angle is given by

$$\tan 2\gamma = \frac{4 v_{\mathbf{h}} v_{\mathbf{s}}}{3v_{\mathbf{s}}^2 - v_{\mathbf{h}}^2 - f^2}. \quad (2.11)$$

The mass eigenvalues are complicated expressions of the parameters appearing in the scalar potential and of the scalar VEVs. Two simple expressions can be found in the limit of  $\alpha, \beta \ll \lambda$  and positive  $\beta$ :

$$m_\sigma^2 \simeq 8\lambda f^2 + 2\beta(3f^2 - v_h^2), \quad m_h^2 \simeq 2\beta v_h^2. \quad (2.12)$$

Although the case  $m_\sigma < m_h$  is parametrically viable, it is a very fine-tuned possibility (see Refs. [6, 36]) and therefore will not be considered here after.

It will be useful in the following to express the different parameters of the scalar potential in terms of the Fermi constant  $G_F$ , the scalar masses, the mixing angles  $\gamma$ :

$$\begin{aligned} v_h^2 &= \frac{1}{\sqrt{2}G_F} & v_s &= \frac{v_h \sin(2\gamma)(m_\sigma^2 - m_h^2)}{m_\sigma^2 + m_h^2 - (m_\sigma^2 - m_h^2)\cos(2\gamma)} \\ \lambda &= \frac{\sin^2 \gamma m_\sigma^2}{8v_h^2} \left(1 + \cot^2 \gamma \frac{m_h^2}{m_\sigma^2}\right) & \frac{\beta}{4\lambda} &= \frac{m_\sigma^2 m_h^2}{\sin^2 \gamma m_\sigma^4 + \cos^2 \gamma m_h^4 - 2m_h^2 m_\sigma^2} \\ \frac{\alpha^2}{4\beta^2} &= \frac{\sin^2(2\gamma)(m_\sigma^2 - m_h^2)^2}{4(\sin^2 \gamma m_\sigma^4 + \cos^2 \gamma m_h^4 - 2m_h^2 m_\sigma^2)} & f^2 &= \frac{v_h^2 (\sin^2 \gamma m_\sigma^4 + \cos^2 \gamma m_h^4 - 2m_h^2 m_\sigma^2)}{(\sin^2 \gamma m_\sigma^2 + \cos^2 \gamma m_h^2)^2}. \end{aligned} \quad (2.13)$$

As  $G_F$  and  $m_h$  are fixed experimentally, the whole set of parameters can be fully determined in terms of only the mass of the extra singlet  $\sigma$  and of its mixing angle with the Higgs. Fig. 1 collects the present bounds on the parameter space  $m_\sigma \times \sin^2 \gamma$ .

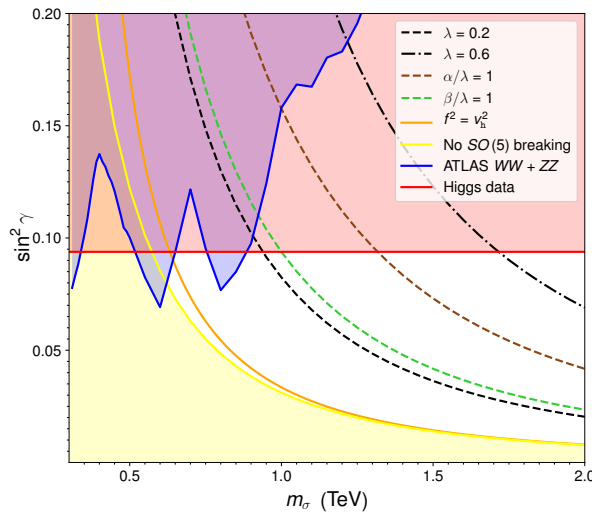


Figure 1: Constraints on the mass ( $m_\sigma$ ) and mixing angle ( $\sin^2 \gamma$ ) of the new singlet scalar  $\sigma$  (see text for details).

The red horizontal line corresponds to an upper bound on  $\sin^2 \gamma$  that universally suppresses the couplings of  $h$  to SM particles with respect to their SM values and it comes from the 125 GeV Higgs signal strengths at the LHC by ATLAS and CMS. Very recent ATLAS results from a  $\sqrt{s} = 13$  TeV analysis of Higgs signal strengths with  $80 \text{ fb}^{-1}$  of integrated luminosity [46] set the bound

$$\sin^2 \gamma \lesssim 0.09 \quad (2.14)$$

at 95% C.L. using a  $\chi^2$  fit to the ATLAS data by assuming a universal suppression of Higgs couplings. The whole red shaded region is then excluded by this data.

The blue region, instead, is the excluded area due to searches of heavy scalars decaying into SM gauge boson pairs. In order to derive this bound, it is useful to introduced an effective Higgs-singlet mixing angle  $\sin^2 \gamma_{\text{eff}}$  as the ratio between the cross sections for gluon fusion production of  $\sigma$  in the ML $\sigma$ M (taking into account the VLQ loop contributions to  $gg \rightarrow \sigma$ , whose expressions can be found in Ref. [6]) and for gluon fusion production of a SM-like scalar  $h_{m_\sigma}$ , with mass  $m_\sigma$

$$\sin^2 \gamma_{\text{eff}} = \frac{\sigma(gg \rightarrow \sigma)_{\text{ML}\sigma\text{M}}}{\sigma(gg \rightarrow h_{m_\sigma})_{\text{SM}}}. \quad (2.15)$$

In the absence of VLQ loop contributions, one simply has  $\sin^2 \gamma_{\text{eff}} = \sin^2 \gamma$ . Considering the latest  $\sqrt{s} = 13$  TeV ATLAS search for scalar resonances in di-boson final states with  $36 \text{ fb}^{-1}$  of integrated luminosity [47], Fig. 1 shows the the 95% C.L. limits in  $\sin^2 \gamma_{\text{eff}}$  as an excluded blue area, in the absence of VLQ loop contributions. The inclusion of the exotic fermion contributions is discussed in Ref. [38].

Finally, Fig. 1 highlights the impact of theoretical constraints on the ML $\sigma$ M parameter space: the area under the yellow curve is ruled out when requiring a feasible spontaneous symmetry breaking of the ML $\sigma$ M  $SO(5)$  group. Note that realisations where  $v_{\text{h}}^2/f^2 \equiv \xi = 1$  (with  $\xi$  the non-linearity parameter typically introduced in CH models), depicted by the orange line, and even regions where  $v_{\text{h}}^2 > f^2$  are not excluded by experimental bounds. The bound from Eq. (2.14) is consistent with existing bounds on  $\xi$  in the non-linear limit  $m_\sigma \gg m_h$ , for which  $\xi \simeq \sin^2 \gamma$  [6]. For completeness, Fig. 1 shows other lines where the  $SO(5)$  preserving parameter  $\lambda$  takes particular values and where it is equal to the remaining parameters of the scalar potential of Eq. (2.2).

## 2.2 The Fermionic Sector

The part of the Lagrangian describing quark interactions can be written as follows [6]

$$\begin{aligned} \mathcal{L}_f = & \bar{\mathbf{q}}_L i \not{D} \mathbf{q}_L + \bar{\mathbf{t}}_R i \not{D} \mathbf{t}_R + \bar{\mathbf{b}}_R i \not{D} \mathbf{b}_R + \\ & + \bar{\psi}^{(2/3)} [i \not{D} - M_5] \psi^{(2/3)} + \bar{\chi}^{(2/3)} [i \not{D} - M_1] \chi^{(2/3)} + \\ & + \bar{\psi}^{(-1/3)} [i \not{D} - M'_5] \psi^{(-1/3)} + \bar{\chi}^{(-1/3)} [i \not{D} - M'_1] \chi^{(-1/3)} + \\ & - \left[ y_1 \bar{\psi}_L^{(2/3)} \phi \chi_R^{(2/3)} + y_2 \bar{\psi}_R^{(2/3)} \phi \chi_L^{(2/3)} + y'_1 \bar{\psi}_L^{(-1/3)} \phi \chi_R^{(-1/3)} + y'_2 \bar{\psi}_R^{(-1/3)} \phi \chi_L^{(-1/3)} + \right. \\ & + \Lambda_1 \left( \bar{\mathbf{q}}_L \Delta_{2 \times 5}^{(2/3)} \psi_R^{(2/3)} \right) + \Lambda_2 \bar{\psi}_L^{(2/3)} \left( \Delta_{5 \times 1}^{(2/3)} \mathbf{t}_R \right) + \Lambda_3 \bar{\chi}_L^{(2/3)} \mathbf{t}_R + \\ & \left. + \Lambda'_1 \left( \bar{\mathbf{q}}_L \Delta_{2 \times 5}^{(-1/3)} \psi_R^{(-1/3)} \right) + \Lambda'_2 \bar{\psi}_L^{(-1/3)} \left( \Delta_{5 \times 1}^{(-1/3)} \mathbf{b}_R \right) + \Lambda'_3 \bar{\chi}_L^{(-1/3)} \mathbf{b}_R + \text{h.c.} \right]. \end{aligned} \quad (2.16)$$

where the  $U(1)_X$  charge of the exotic fermion fields  $\psi$  and  $\chi$  has been made explicit throughout. The one associated to the charged lepton is very similar to the down-quark

one with exotic fermions having  $U(1)_X = -1$ . Canonical kinetic terms for the elementary quarks appear in the first line, where  $\mathbf{q}_L$  for the left-handed (LH)  $SU(2)_L$ -doublet,  $\mathbf{t}_R$  and  $\mathbf{b}_R$  for the RH  $SU(2)_L$  singlets. The second and third lines describe the kinetic and mass terms for the exotic quarks. The fourth line presents the proto-Yukawa interactions between the exotic quarks and the scalar quintuplet  $\phi$ . The last two lines contain the mixed terms describing the elementary-exotic quark interactions: those terms proportional to  $\Lambda_{1,2}^{(\prime)}$  explicitly break the  $SO(5)$  symmetry and the spurions [48–52]  $\Delta_{2\times 5}$  and  $\Delta_{5\times 1}$  are introduced to formally restore the  $SO(5)$  invariance:

$$\begin{aligned}\Delta_{2\times 5}^{(2/3)} &= \begin{pmatrix} 0 & 0 & 1 & 0 & 0 \\ 0 & 0 & 0 & 1 & 0 \end{pmatrix}, \\ \Delta_{2\times 5}^{(-1/3)} &= \begin{pmatrix} 1 & 0 & 0 & 0 & 0 \\ 0 & 1 & 0 & 0 & 0 \end{pmatrix}, \\ \Delta_{5\times 1}^{(2/3),(-1/3)} &= (0 \ 0 \ 0 \ 0 \ 1)^T.\end{aligned}\tag{2.17}$$

According to the fermion partial compositeness paradigm no direct elementary fermion couplings to  $\phi$  are allowed. Notice that for these couplings to be added in the previous fermionic Lagrangian new spurion fields should be introduced and therefore the model would be less minimal in this case.

The direct masses  $M_{1,5}^{(\prime)}$  can be taken as real parameters: indeed, if they were complex, then the sum between the mass terms and their hermitian conjugates would end up with the real part of the mass parameters. On the other side, the rest of parameters should be taken as complex:  $y_{1,2}^{(\prime)} = |y_{1,2}^{(\prime)}| e^{i\alpha_{1,2}^{(\prime)}}$  and  $\Lambda_{1,2,3}^{(\prime)} = |\Lambda_{1,2,3}^{(\prime)}| e^{i\beta_{1,2,3}^{(\prime)}}$ . Performing a field redefinition is possible to reduce the number of phases to the minimum set of 4 phases: a possible choice is

$$\begin{aligned}\psi_{L,R}^{(2/3)} &\implies e^{-i\beta_1} \psi_{L,R}^{(2/3)}, & \psi_{L,R}^{(-1/3)} &\implies e^{-i\beta'_1} \psi_{L,R}^{(-1/3)}, \\ \mathbf{t}_R &\implies e^{-i(\beta_1+\beta_2)} \mathbf{t}_R, & \mathbf{b}_R &\implies e^{-i(\beta'_1+\beta'_2)} \mathbf{b}_R, \\ \chi_{L,R}^{(2/3)} &\implies e^{i(\beta_3-\beta_2-\beta_1)} \chi_{L,R}^{(2/3)}, & \chi_{L,R}^{(-1/3)} &\implies e^{i(\beta'_3-\beta'_2-\beta'_1)} \chi_{L,R}^{(-1/3)},\end{aligned}\tag{2.18}$$

leaving only  $y_{1,2}^{(\prime)}$  as complex parameters. Notice that  $\psi_L$  and  $\psi_R$  ( $\chi_L$  and  $\chi_R$ ) transform identically to not introduce any phase in the mass terms. Among the elementary fields, only the RH quarks transform and in particular  $\mathbf{q}_L$  is not redefined to avoid mixing the phases between the up and down sectors and in order not to introduce any additional phase to the SM gauge boson couplings.

It is useful to rewrite the expression in Eq. (2.16) in terms of the  $SU(2)_L$  components of the different fields:

$$\begin{aligned}\phi &= (H^T, \tilde{H}^T, \mathbf{s}), \\ \psi^{(2/3)} &\sim (\mathbf{K}, \mathbf{Q}, \mathbf{T}_5)^T, & \chi^{(2/3)} &\sim \mathbf{T}_1, \\ \psi^{(-1/3)} &\sim (\mathbf{Q}', \mathbf{K}', \mathbf{B}_5)^T, & \chi^{(-1/3)} &\sim \mathbf{B}_1,\end{aligned}\tag{2.19}$$

where  $H$  is the SM  $SU(2)_L$  doublet, with  $\tilde{H} \equiv i\sigma_2 H^*$ , and  $\mathbf{K}^{(\prime)}$  and  $\mathbf{Q}^{(\prime)}$  are  $SU(2)_L$  doublets and  $\mathbf{T}_{1,5}$  and  $\mathbf{B}_{1,5}$  are singlets. The whole set of charge assignments can be read in Tab. 2,

where the hypercharge is defined as

$$Y = \Sigma_R^{(3)} + X, \quad (2.20)$$

with  $X$  the  $U(1)_X$  charge and  $\Sigma_R^{(3)}$  the third component of the global  $SU(2)_R$ , which is part of the residual  $SO(4)$  group after the breaking of  $SO(5)$ .

Charge/Field	K	Q	$T_{1,5}$	Q'	K'	$B_{1,5}$
$\Sigma_R^{(3)}$	+1/2	-1/2	0	+1/2	-1/2	0
$SU(2)_L \times U(1)_Y$	(2, +7/6)	(2, +1/6)	(1, +2/3)	(2, +1/6)	(2, -5/6)	(1, -1/3)
$U(1)_X$	+2/3	+2/3	+2/3	-1/3	-1/3	-1/3
$U(1)_{EM}$	$K^u = +5/3$ $K^d = +2/3$	$Q^u = +2/3$ $Q^d = -1/3$	+2/3	$Q'^u = +2/3$ $Q'^d = -1/3$	$K'^u = -1/3$ $K'^d = -4/3$	-1/3

Table 2: *Decompositions of the exotic quarks and their transformations under the SM group.*

By using Eqs. (2.17) and (2.19), Eq. (2.16) acquires the following form

$$\begin{aligned}
\mathcal{L}_f = & \bar{q}_L i\not{D} q_L + \bar{\tau}_R i\not{D} \tau_R + \bar{b}_R i\not{D} b_R + \\
& + \bar{K} [i\not{D} - M_5] K + \bar{Q} [i\not{D} - M_5] Q + \bar{T}_5 [i\not{D} - M_5] T_5 + \bar{T}_1 [i\not{D} - M_1] T_1 + \\
& + \bar{Q}' [i\not{D} - M'_5] Q' + \bar{K}' [i\not{D} - M'_5] K' + \bar{B}_5 [i\not{D} - M'_5] B_5 + \bar{B}_1 [i\not{D} - M'_1] B_1 + \\
& - \left[ y_1 \left( \bar{K}_L H T_{1,R} + \bar{Q}_L \tilde{H} T_{1,R} + \bar{T}_{5,L} \mathbf{s} T_{1,R} \right) + y_2 \left( \bar{T}_{1,L} H^\dagger K_R + \bar{T}_{1,L} \tilde{H}^\dagger Q_R + \bar{T}_{1,L} \mathbf{s} T_{5,R} \right) \right] + \\
& + y'_1 \left( \bar{Q}'_L H B_{1,R} + \bar{K}'_L \tilde{H} B_{1,R} + \bar{B}_{5,L} \mathbf{s} B_{1,R} \right) + y'_2 \left( \bar{B}_{1,L} H^\dagger Q'_R + \bar{B}_{1,L} \tilde{H}^\dagger K'_R + \bar{B}_{1,L} \mathbf{s} B_{5,R} \right) + \\
& + \Lambda_1 \bar{q}_L Q_R + \Lambda_2 \bar{T}_{5,L} \tau_R + \Lambda_3 \bar{T}_{1,L} \tau_R + \Lambda'_1 \bar{q}_L Q'_R + \Lambda'_2 \bar{B}_{5,L} b_R + \Lambda'_3 \bar{B}_{1,L} b_R + \text{h.c.} \Big], \quad (2.21)
\end{aligned}$$

where the scalar fields  $H$  and  $\mathbf{s}$  still denote the unshifted and unrotated fields defined in Eq. (2.1). In order to match with the notation adopted in the previous section, notice that in the unitary gauge

$$H \equiv \begin{pmatrix} 0 \\ h/\sqrt{2} \end{pmatrix}. \quad (2.22)$$

Fermion masses and mixings arise by diagonalising the whole fermion mass matrix that includes elementary and exotic quarks. To this end, all fermions can be grouped together in a single vector

$$\Psi = (K^u, \mathcal{T}, \mathcal{B}, K'^d)^T, \quad (2.23)$$

where the ordering of the components is based on their electric charges, +5/3, +2/3, -1/3, and -4/3, respectively. Notice that  $\mathcal{T}$  and  $\mathcal{B}$  list together all the states with same electric charge, +2/3 and -1/3, respectively,

$$\begin{aligned}
\mathcal{T} &= (\tau, Q^u, K^d, T_5, T_1, Q'^u)^T, \\
\mathcal{B} &= (b, Q'^d, K^u, B_5, B_1, Q^d)^T.
\end{aligned} \quad (2.24)$$

The whole fermion mass term can then be written in the interaction basis as

$$\mathcal{L}_{\mathcal{M}} = -\bar{\Psi}_L \mathcal{M}(v_h, v_s) \Psi_R, \quad (2.25)$$

where the mass matrix  $\mathcal{M}(v_h, v_s)$  is a  $14 \times 14$  block diagonal matrix,

$$\mathcal{M}(v_h, v_s) = \text{diag}\left(M_5, \mathcal{M}_{\mathcal{T}}(v_h, v_s), \mathcal{M}_{\mathcal{B}}(v_h, v_s), M'_5\right), \quad (2.26)$$

with

$$\mathcal{M}_{\mathcal{T}}(v_h, v_s) = \begin{pmatrix} 0 & \Lambda_1 & 0 & 0 & 0 & \Lambda'_1 \\ 0 & M_5 & 0 & 0 & y_1 \frac{v_h}{\sqrt{2}} & 0 \\ 0 & 0 & M_5 & 0 & y_1 \frac{v_h}{\sqrt{2}} & 0 \\ \Lambda_2 & 0 & 0 & M_5 & y_1 v_s & 0 \\ \Lambda_3 & y_2 \frac{v_h}{\sqrt{2}} & y_2 \frac{v_h}{\sqrt{2}} & y_2 v_s & M_1 & 0 \\ 0 & 0 & 0 & 0 & 0 & M'_5 \end{pmatrix}, \quad (2.27)$$

and similarly for  $\mathcal{M}_{\mathcal{B}}(v_h, v_s)$ , replacing the unprimed parameters with the primed ones and vice-versa.

The matrix in Eq. (2.26) can be diagonalised through a bi-unitary transformation,

$$\widehat{\Psi}_{L,R} = U_{L,R} \Psi \quad \Longrightarrow \quad \widehat{\mathcal{M}} = U_L \mathcal{M} U_R^\dagger, \quad (2.28)$$

where  $\widehat{\Psi}_{L,R}$  stand for the mass eigenstates and  $\widehat{\mathcal{M}}$  for the diagonal matrix. The two unitary matrices can be written as block-diagonal structures

$$U_{L,R} = \text{diag}\left(1, U_{L,R}^{\mathcal{T}}, U_{L,R}^{\mathcal{B}}, 1\right), \quad (2.29)$$

where  $U_{L,R}^{\mathcal{T}}$  and  $U_{L,R}^{\mathcal{B}}$  diagonalise  $\mathcal{M}_{\mathcal{T}}(v_h, v_s)$  and  $\mathcal{M}_{\mathcal{B}}(v_h, v_s)$ , respectively. Finally, the diagonalised mass matrix is given by

$$\widehat{\mathcal{M}} = \text{diag}\left(M_5, \widehat{\mathcal{M}}_{\mathcal{T}}, \widehat{\mathcal{M}}_{\mathcal{B}}, M'_5\right) \quad (2.30)$$

and the mass eigenstate fermion fields are defined as

$$\begin{aligned} \widehat{\Psi} &= \left(K^u, \widehat{\mathcal{T}}, \widehat{\mathcal{B}}, K^{td}\right)^T, \\ \widehat{\mathcal{T}} &= (t, T, T_2, T_3, T_4, T_5)^T, \\ \widehat{\mathcal{B}} &= (b, B, B_2, B_3, B_4, B_5)^T, \end{aligned} \quad (2.31)$$

with both charge  $2/3$  and charge  $-1/3$  mass eigenstates ordered by increasing masses, so that the lightest states correspond to the top and bottom quarks, respectively. Notice that the exotic charge states do not mix with the other fields and then  $K^u \equiv K^u$  and  $K^{td} \equiv K^{td}$ .

The final expression for the tree level top quark mass is given by

$$m_t = \frac{y_1 \Lambda_1 \Lambda_3 v_h / \sqrt{2}}{M_1 M_5 - y_1 y_2 (v_h^2 + v_s^2)} - \frac{y_1 y_2 \Lambda_1 \Lambda_2 v_s v_h / \sqrt{2}}{M_1 M_5^2 - y_1 y_2 M_5 (v_h^2 + v_s^2)}, \quad (2.32)$$

and similarly for the bottom quark mass, replacing the unprimed parameters with the primed ones.

Ref. [38] contains a comprehensive study of the model phenomenology addressing in particular the effects of relatively light top and bottom partners. This analysis includes the study of the modification of the  $Z\bar{b}b$  coupling having an impact on the ratios of partial widths  $R_b = \Gamma(Z \rightarrow \bar{b}b)/\Gamma(Z \rightarrow \text{hadrons})$ ,  $R_c = \Gamma(Z \rightarrow \bar{c}c)/\Gamma(Z \rightarrow \text{hadrons})$ , on the forward-backward charge asymmetry  $A_{FB}^b$  and on the coupling  $A^b$  from left-right forward-backward asymmetry. Bounds from  $S$  and  $T$  oblique parameters have also been considered and a series of benchmarks have been identified where the parameter space pass all these constraints. For each benchmark, the branching ratio of the lightest top and bottom partners to top and bottom quark and the heavy singlet  $\sigma$  have been studied, finding that these decays may be dominant and provide interesting signals at colliders.

## 2.3 The Low-Energy Effective Operators

A common procedure to analyse the contributions to the electron EDM consists in computing the low-energy Lagrangian of the model integrating out the heaviest dofs and matching to Eq. (1.3). This limit corresponds to consider  $M \gg m_\sigma \gg v_h$ , where  $M$  generically represents the exotic fermion mass scales  $M_i^{(\prime)}$  in Eq. (2.16). Generically, the GB scale  $f$  is smaller than  $M$  and therefore the additional expansion  $f/M \ll 1$  will be also considered; on the contrary, the scales  $\Lambda_i^{(\prime)}$  can be taken of the same order of magnitude of  $M$ . This integration out exercise has already been carried out in Ref. [6], but without considering complex parameters: this section is devoted to reproducing the results in that paper, but taking trace of the CPV sources.

For energies  $E < M$ , the effective Lagrangian describing  $d \leq 6$  operators containing SM quarks interactions with gauge bosons, Higgs and  $\sigma$  can be written as

$$\mathcal{L}_{\text{eff}} = \bar{q}_L i\not{D} q_L + \bar{t}_R i\not{D} t_R + \bar{b}_R i\not{D} b_R + \sum_{i, c_i \in \mathbb{R}} c_i \mathcal{O}_i + \left( \sum_{j, c_j \in \mathbb{C}} c_j \mathcal{O}_j + \text{h.c.} \right). \quad (2.33)$$

For concreteness, the ‘‘Warsaw basis’’ [53] will be used and charged lepton operators will not be shown explicitly.

The light fermion kinetic energies also receive contributions that requires wave function renormalisation in order to recover canonically normalised kinetic terms,

$$\begin{aligned} q_L &\rightarrow \mathcal{Z}_{q_L}^{-1/2} q_L & \text{with} & \quad \mathcal{Z}_{q_L} = 1 + \frac{\Lambda_1^2}{M_5^2} + \frac{\Lambda_1'^2}{M_5'^2} \\ t_R &\rightarrow \mathcal{Z}_{t_R}^{-1/2} t_R & \text{with} & \quad \mathcal{Z}_{t_R} = 1 + \frac{\Lambda_2^2}{M_5^2} + \frac{\Lambda_3^2}{M_1^2} \\ b_R &\rightarrow \mathcal{Z}_{b_R}^{-1/2} b_R & \text{with} & \quad \mathcal{Z}_{b_R} = 1 + \frac{\Lambda_2'^2}{M_5'^2} + \frac{\Lambda_3'^2}{M_1'^2}. \end{aligned} \quad (2.34)$$

The low-energy operators obtained and their coefficients at leading order in  $f/M$  are

$d$	Operator	$c_i$	Leading Order in $f/M$
4	$\bar{q}_L \tilde{H} t_R$	$-Y_t$	$-\left(\frac{y_1 \Lambda_1 \Lambda_3}{M_1 M_5}\right) \mathcal{Z}_{q_L}^{-1/2} \mathcal{Z}_{t_R}^{-1/2}$
	$\bar{q}_L H b_R$	$-Y_b$	$-\left(\frac{y'_1 \Lambda'_1 \Lambda'_3}{M'_1 M'_5}\right) \mathcal{Z}_{q_L}^{-1/2} \mathcal{Z}_{b_R}^{-1/2}$
5	$\mathbf{s}(\bar{q}_L \tilde{H} t_R)$	$c_{\mathbf{s}1}^t$	$\frac{Y_t}{M_5} \left[ y_2^* \frac{\Lambda_2}{\Lambda_3} - \left( y_1 \frac{\Lambda_2 \Lambda_3}{M_1 M_5} + y_2^* \frac{\Lambda_2 \Lambda_3}{M_1^2} \right) \mathcal{Z}_{t_R}^{-1} \right]$
	$\mathbf{s}(\bar{q}_L H b_R)$	$c_{\mathbf{s}1}^b$	$\frac{Y_b}{M'_5} \left[ y_2'^* \frac{\Lambda'_2}{\Lambda'_3} - \left( y'_1 \frac{\Lambda'_2 \Lambda'_3}{M'_1 M'_5} + y_2'^* \frac{\Lambda'_2 \Lambda'_3}{M_1'^2} \right) \mathcal{Z}_{b_R}^{-1} \right]$
6	$\mathbf{s}^2(\bar{q}_L \tilde{H} t_R)$	$c_{\mathbf{s}2}^t$	$-\frac{Y_t}{M_1 M_5} \left\{ y_1 y_2^* - \left[ y_1 y_2^* \left( 2 \frac{\Lambda_2^2}{M_5^2} + \frac{\Lambda_3^2}{M_1^2} \right) + \frac{( y_2 ^2 + 2y_2^{*2})\Lambda_2^2 +  y_1 ^2 \Lambda_3^2}{2M_1 M_5} \right] \mathcal{Z}_{t_R}^{-1} + \right.$ $\left. + 2 \frac{\Lambda_2^2 \Lambda_3^2}{M_1 M_5} \left( \frac{y_1 \text{Re}[y_1]}{M_5^2} + \frac{y_1 \text{Re}[y_2] + y_2^* \text{Re}[y_1]}{M_5 M_1} + \frac{y_2^* \text{Re}[y_2]}{M_1^2} \right) \mathcal{Z}_{t_R}^{-2} \right\}$
	$\mathbf{s}^2(\bar{q}_L H b_R)$	$c_{\mathbf{s}2}^b$	$-\frac{Y_b}{M'_1 M'_5} \left\{ y'_1 y_2'^* - \left[ y'_1 y_2'^* \left( 2 \frac{\Lambda_2'^2}{M_5'^2} + \frac{\Lambda_3'^2}{M_1'^2} \right) + \frac{( y_2' ^2 + 2y_2'^{*2})\Lambda_2'^2 +  y_1' ^2 \Lambda_3'^2}{2M'_1 M'_5} \right] \mathcal{Z}_{b_R}^{-1} + \right.$ $\left. + 2 \frac{\Lambda_2'^2 \Lambda_3'^2}{M'_1 M'_5} \left( \frac{y'_1 \text{Re}[y'_1]}{M_5'^2} + \frac{y'_1 \text{Re}[y'_2] + y_2'^* \text{Re}[y'_1]}{M_5' M_1'} + \frac{y_2'^* \text{Re}[y'_2]}{M_1'^2} \right) \mathcal{Z}_{b_R}^{-2} \right\}$
	$ H ^2(\bar{q}_L \tilde{H} t_R)$	$c_{H2}^t$	$-\frac{Y_t}{M_1 M_5} \left[ 2y_1 y_2^* - \left( 2y_1 y_2^* \frac{\Lambda_3^2}{M_1^2} +  y_1 ^2 \frac{\Lambda_3^2}{M_1 M_5} \right) \mathcal{Z}_{t_R}^{-1} - \left( y_1 y_2^* \frac{\Lambda_1^2}{M_5^2} + \frac{ y_1 ^2}{2} \frac{\Lambda_1^2}{M_1 M_5} \right) \mathcal{Z}_{q_L}^{-1} \right]$
	$ H ^2(\bar{q}_L H b_R)$	$c_{H2}^b$	$-\frac{Y_b}{M'_1 M'_5} \left[ 2y'_1 y_2'^* - \left( 2y'_1 y_2'^* \frac{\Lambda_3'^2}{M_1'^2} +  y_1' ^2 \frac{\Lambda_3'^2}{M_1' M'_5} \right) \mathcal{Z}_{b_R}^{-1} - \left( y'_1 y_2'^* \frac{\Lambda_1'^2}{M_5'^2} + \frac{ y_1' ^2}{2} \frac{\Lambda_1'^2}{M_1' M'_5} \right) \mathcal{Z}_{q_L}^{-1} \right]$
	$(H^\dagger i \overleftrightarrow{D}_\mu H)(\bar{q}_L \gamma^\mu q_L)$	$c_L^{(1)}$	$\frac{1}{4} \left( \frac{ y_1 ^2 \Lambda_1^2}{M_1^2 M_5^2} - \frac{ y_1' ^2 \Lambda_1'^2}{M_1'^2 M_5'^2} \right) \mathcal{Z}_{q_L}^{-1}$
	$(H^\dagger i \overleftrightarrow{D}_\mu^i H)(\bar{q}_L \tau^i \gamma^\mu q_L)$	$c_L^{(3)}$	$-\frac{1}{4} \left( \frac{ y_1 ^2 \Lambda_1^2}{M_1^2 M_5^2} + \frac{ y_1' ^2 \Lambda_1'^2}{M_1'^2 M_5'^2} \right) \mathcal{Z}_{q_L}^{-1}$

Table 3: Leading order low-energy effective operators and their coefficients. The wave function renormalisation factors have been defined in Eq. (2.34).

shown in Tab. 3, where the following definitions are being used:

$$\begin{aligned} (H^\dagger i \overleftrightarrow{D}_\mu H) &\equiv i \left( H^\dagger \left( \overrightarrow{D}_\mu H \right) - \left( H^\dagger \overleftarrow{D}_\mu \right) H \right), \\ (H^\dagger i \overleftrightarrow{D}_\mu^i H) &\equiv i \left( H^\dagger \tau^i \left( \overrightarrow{D}_\mu H \right) - \left( H^\dagger \overleftarrow{D}_\mu \right) \tau^i H \right). \end{aligned} \quad (2.35)$$

Moreover the symbol  $\text{Re}[x]$  refers to the real part of the parameter  $x$ . Notice that the coefficients of the  $d = 4$  operators also enter in the definition of the higher dimensional operator coefficients.

The Yukawas  $Y_t$  and  $Y_b$  do not lead to the top and bottom masses: on one hand, they are proportional to  $y_1^{(\prime)}$  that are complex; on the other hand, the Yukawa operators receive contributions from operators of higher dimensions once the scalar fields  $H$  and  $\mathbf{s}$  develop their VEVs. The latter contributions are additionally suppressed by powers of  $f/M$  and therefore can be safely neglected at the approximation considered. However, the complex phases entering  $Y_t$  and  $Y_b$  need to be reabsorbed. By redefining the fields  $t_R$  and  $b_R$  such that

$$t_R \rightarrow e^{-i\alpha_1} t_R, \quad b_R \rightarrow e^{-i\alpha'_1} b_R, \quad (2.36)$$

then

$$Y_t \rightarrow |Y_t| \equiv y_t, \quad Y_b \rightarrow |Y_b| \equiv y_b, \quad (2.37)$$

and the top and bottom masses at leading order in  $f/M$  turn out to be

$$m_t = \frac{|y_1| \Lambda_1 \Lambda_3 v_h}{\sqrt{2} M_1 M_5} \mathcal{Z}_{q_L}^{-1/2} \mathcal{Z}_{t_R}^{-1/2}, \quad m_b = \frac{|y'_1| \Lambda'_1 \Lambda'_3 v_h}{\sqrt{2} M'_1 M'_5} \mathcal{Z}_{q_L}^{-1/2} \mathcal{Z}_{b_R}^{-1/2}. \quad (2.38)$$

These redefinitions also affect the other operators in Tab. 3 such that in the coefficients  $c_{s1}^{t,b}$ ,  $c_{s2}^{t,b}$  and  $c_{H2}^{t,b}$ , the couplings  $Y_t$  and  $Y_b$  should be replaced by their absolute value counterparts  $y_t$  and  $y_b$ , respectively. Since  $y_1^{(\prime)}$  and  $y_2^{(\prime)}$  within these coefficients are complex, the new sources of CPV have not been washed out by the redefinition in Eq. (2.36).

As for the Yukawa couplings, the  $d = 5$  coefficients receive contributions from higher dimension operators, but they are suppressed by powers of  $f/M$  and therefore safely negligible in the approximation considered here. The  $d = 5$  operators mainly contribute to electron EDM and will be the focus of the next section.

### 3 The Electric Dipole Moment

The electron EDM prediction within the  $\text{ML}\sigma\text{M}$  deviates from the SM one due to the contributions originated from the exotic fields present in the spectrum. Eq. (1.3) parametrises the light fermion couplings to the SM Higgs:  $\kappa_\psi$  is the CP conserving coefficient, while  $\tilde{\kappa}_\psi$  is the CPV one. Within the SM,  $\kappa_\psi = 1$  while  $\tilde{\kappa}_\psi = 0$  for any light fermion  $\psi$ . Once the latter coefficient is different from zero, then a new contribution to the electron EDM arises through the so-called Barr-Zee diagram in Fig. 2. The different vertices are labelled with letters: the vertexes “B”, “D” and “E” are purely SM as the photon couplings are left untouched within the  $\text{ML}\sigma\text{M}$ ; the vertex “A” is also taken to be SM-like, as already discussed, because the lighter fermion generations receive the smallest,

and therefore negligible, contributions in the fermion partial compositeness mechanism; the only vertex where NP can play a role is “C”. It follows that only  $h$  can mediate this process and not  $\sigma$ , whose couplings with electrons are taken to be vanishing.

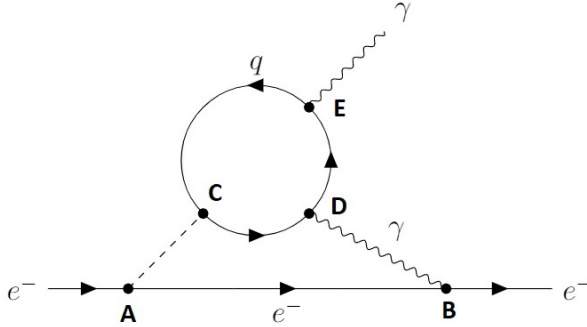


Figure 2: *Two-loop Barr-Zee diagram for the electron EDM.*

The explicit computation of the Barr-Zee diagram, allowing NP only in the vertex “C”, provides the following contribution to the electron EDM [39]:

$$\frac{d_e}{e} = - \sum_{\psi=t,b,\tau} 4 Q_e Q_\psi^2 N_c \frac{\alpha_{\text{em}}}{(4\pi)^3} \sqrt{2} G_F m_e \kappa_e \tilde{\kappa}_\psi f_1(x_\psi), \quad (3.1)$$

where  $Q_\psi$  is the  $\psi$  electric charge,  $N_c = 3$  if  $\psi$  is a quark and  $N_c = 1$  if  $\psi$  is the  $\tau$ ,  $\alpha_{\text{em}}$  is the fine structure constant at the scale of the electron mass,  $G_F$  the Fermi constant, and  $f_1$  is a function of  $x_\psi \equiv (m_\psi/m_h)^2$  defined by

$$f_1(x) = \frac{2x}{\sqrt{1-4x}} \left[ \text{Li}_2 \left( 1 - \frac{1 - \sqrt{1-4x}}{2x} \right) - \text{Li}_2 \left( 1 - \frac{1 + \sqrt{1-4x}}{2x} \right) \right] \quad (3.2)$$

being  $\text{Li}_2$  the dilogarithm

$$\text{Li}_2(z) = - \int_0^1 \frac{\ln(1-zt)}{t} dt, \quad z \in \mathbb{C}, \quad t \in \mathbb{R}. \quad (3.3)$$

The numerical results for the function  $f_1$  computed for the top, bottom and  $\tau$  fermions are such that  $f_1(x_t) \simeq 2.87$ ,  $f_1(x_b) \simeq 0.055$  and  $f_1(x_\tau) \simeq 0.015$ , taking the central experimental values for the fermion masses,  $m_t = 172.8$  GeV,  $m_b = 4.18$  GeV and  $m_\tau = 1.78$  GeV, and the Higgs mass as  $m_h = 125.1$  GeV [1]. These values have been obtained implementing in C++ the sub-routine Vegas [54] from the Monte Carlo-based multi-dimensional Cuba library [55].

Assuming one contribution at the time, from Eq. (3.1) and the obtained values for  $f_1$  and using the experimental bound in Eq. (1.1), one obtains the upper bounds on  $\tilde{\kappa}_t$ ,  $\tilde{\kappa}_b$ ,  $\tilde{\kappa}_\tau$ ,

$$\tilde{\kappa}_t = 0.0012, \quad \tilde{\kappa}_b = 0.24, \quad \tilde{\kappa}_\tau = 0.3, \quad (3.4)$$

in agreement with the values for  $T_I^\psi$  in Ref. [40] (see their Eq. (4.5)), satisfying

$$T_I^\psi = \frac{\tilde{\kappa}_\psi}{3}. \quad (3.5)$$

It follows that the bound on  $\tilde{\kappa}_t$  is almost two orders of magnitude stronger than on  $\tilde{\kappa}_b$  and  $\tilde{\kappa}_\tau$ , so only that will be considered hereafter.

In the next step we can express  $\tilde{\kappa}_t$  in terms of the Lagrangian parameters of the model. To this end one can explicitly go to the scalar mass basis when writing the  $d = 5$  operators in Tab. 3: recalling the relations in Eq. (2.10), it follows

$$c_{s1}^t \mathbf{s} (\bar{q}_L \tilde{H} t_R) + \text{h.c.} \supset \frac{v_s \cos \gamma - v_h \sin \gamma}{\sqrt{2}} \text{Re}[c_{s1}^t] h \bar{t} t + i \frac{v_s \cos \gamma - v_h \sin \gamma}{\sqrt{2}} \text{Im}[c_{s1}^t] h \bar{t} \gamma_5 t, \quad (3.6)$$

where  $\text{Im}[x]$  is the imaginary part of  $x$ , and where in the right-hand side only the couplings with the physical Higgs  $h$  are retained. Comparing this expression with the one in Eq. (1.3), it is possible to read the values of  $\tilde{\kappa}_t$ :

$$\tilde{\kappa}_t = (v_h \sin \gamma - v_s \cos \gamma) \text{Im} \left[ \frac{1}{M_5} \left( y_2^* \frac{\Lambda_2}{\Lambda_3} - \left( y_1 \frac{\Lambda_2 \Lambda_3}{M_1 M_5} + y_2^* \frac{\Lambda_2 \Lambda_3}{M_1^2} \right) \mathcal{Z}_{tR}^{-1} \right) \right]. \quad (3.7)$$

### 3.1 Numerical Results

Given the upper bound on  $\tilde{\kappa}_t$  we are interested in obtaining some information about the range of acceptable phase values in the couplings  $y$ 's. Since the number of mass parameters in the model is large, a series of benchmarks have been selected for the parameters entering Eq. (3.7): the upper part of Tab. 4 reports the input parameters for each of the benchmark considered, while some relevant phenomenological feature is collected in the bottom part of it. Notice that  $y_2'$  is always taken to be vanishing to simplify the discussion: a non-vanishing value for this parameter does not change the core of the analysis. Moreover, the elements  $V_{Tb,tB}^{L,R}$  and  $X_{tT,bB}^{L,R}$  are defined as the couplings with the SM EW gauge bosons,

$$\begin{aligned} \mathcal{L}_{WQq} &= \frac{g}{\sqrt{2}} \left[ \bar{T} \gamma^\mu (V_{Tb}^L P_L + V_{Tb}^R P_R) b + \bar{t} \gamma^\mu (V_{tB}^L P_L + V_{tB}^R P_R) B \right] W_\mu^+ + \text{h.c.}, \\ \mathcal{L}_{ZQq} &= \frac{g}{2c_W} \left[ \bar{t} \gamma^\mu (X_{tT}^L P_L + X_{tT}^R P_R) T - \bar{b} \gamma^\mu (X_{bB}^L P_L + X_{bB}^R P_R) B \right] Z_\mu + \text{h.c.} \end{aligned} \quad (3.8)$$

The branching ratios refer to the lightest exotic fermion decays in the final states indicated in the table. The horizontal lines correspond to not reported values as in those cases the quark partner is not the lightest one and therefore its phenomenology is not the dominant one.

Each benchmark satisfies to the following list of requirements:

- consistency of the electroweak precision observables
- consistency of  $R_b$ ,  $R_c$ ,  $A_{FB}^b$  and  $A^b$  due to modification of the  $Z\bar{b}b$ -coupling
- consistency of the Higgs couplings with the SM particles
- searches of heavy scalars decaying into SM gauge boson pairs
- reproduction of  $m_t$  and  $m_b$  (the reproduction of  $m_\tau$  does not affect the EDM computation).

	$m_\sigma$ (TeV)	$\sin^2 \gamma$	$M_1$ (TeV)	$M_5$ (TeV)	$M'_1$ (TeV)	$M'_5$ (TeV)	$\Lambda_1$ (TeV)	$\Lambda_2$ (TeV)	$\Lambda_3$ (TeV)	$\Lambda'_1$ (TeV)	$\Lambda'_2$ (TeV)	$\Lambda'_3$ (TeV)	$ y_1 $	$ y_2 $	$ y'_1 $	$ y'_2 $
P1	0.7	0.08	2.3	4.6	1.6	1.8	8.7	0.5	1.2	0.6	0.4	0.9	2.4	0	0.3	0
P2	0.7	0.08	1.1	6.5	4.6	7.0	9.8	2.7	3.3	0.9	0.8	0.9	1.3	4.9	1.8	0
P3	0.7	0.08	3.8	6.1	4.3	6.5	9.2	1.1	3.5	0.9	0.5	0.8	1.8	5.4	1.9	0

	$m_B$ (TeV)	$m_T$ (TeV)	$ X_{bB}^L $	$ X_{bB}^R $	$ V_{Tb}^L $	$ V_{Tb}^R $	$BR$ ( $\sigma b$ )	$BR$ ( $hb$ )	$BR$ ( $Zb$ )	$BR$ ( $Wt$ )	$BR$ ( $\sigma t$ )	$BR$ ( $ht$ )	$BR$ ( $Zt$ )	$BR$ ( $Wb$ )
P1	1.6	1.8	0.004	0	–	–	0.72	0.07	0.07	0.14	–	–	–	–
P2	4.5	1.7	–	–	0.031	0	–	–	–	–	0.52	0.10	0.13	0.25
P3	4.2	3.2	–	–	0.049	0	–	–	–	–	0.27	0.16	0.20	0.37

Table 4: In the upper panel, three different sets of input parameters are shown as examples, approximating the numerical values at the first relevant digits. The example in the first line illustrates the case with a lightest  $B$  quark partner, while the other two examples the case in which the  $T$  quark partner is the lightest VLQ. The corresponding lightest  $B$  and  $T$  quark partner masses and the single production couplings and branching ratios of the lightest VLQ are collected in the lower panel. The horizontal lines correspond to not reported values as in those cases the quark partner is not the lightest one.

The first line in the panels above corresponds to P1, that is the case in which the  $B$  quark partner is the lightest exotic fermion. The most salient feature is the large branching ratio  $BR(B \rightarrow \sigma b)$  that is actually possible in wide region of the parameter space (see Ref. [38]). This BR can easily be the dominant one in general and it is so for the selected P1 benchmark. For the value of  $X_{bB}^L$  and  $m_B$ , the dominant production process is the pair production  $pp \rightarrow B\bar{B}$  whose cross section is much larger than the one of the single  $B$  production, mainly provided by  $pp \rightarrow B\bar{b}q$  and  $pp \rightarrow \bar{B}bq$ .

The second two lines in the panels in Tab. 4 illustrate two benchmarks, P2 and P3, where the lightest exotic fermion is the  $T$  partner. The main difference between P2 and P3 is  $m_T$ : in these benchmarks, the larger is the mass the smaller is the  $BR(T \rightarrow \sigma t)$ . The latter is dominant in P2, while the dominant branching ratio for P3 is for  $T \rightarrow W^+b$ . Interestingly, the mixing of  $T$  with the SM bottom quark, measured by  $V_{Tb}^L$ , can be much larger than the equivalent in P1: it follows that the single  $T$  production, via the processes  $pp \rightarrow T\bar{b}q$  and  $pp \rightarrow \bar{T}bq$ , may dominate over the pair production. For the values of  $V_{Tb}^L$  and  $m_T$  in P3, this is the case. Notice that this is anti-correlated with the presence of a large  $BR(T \rightarrow \sigma t)$ : for large mixing the branching ratio  $T \rightarrow \sigma t$  is smaller, and vice-versa.

Ref. [38] has provided a detailed analysis of possible discovery of  $T$  and  $B$  partners at colliders and we refer to that publications for such details.

For each benchmark point, the parameter space associated to the physical phases present in the ML $\sigma$ M is constrained by the upper bound for  $\tilde{\kappa}_t$  as shown in Fig. 3. In the plot (a), the benchmark P1 is illustrated, where only  $y_1 \neq 0$ . Plots (b) and (c) refer to P2, taking in each case only one phase different from zero at a time. Plots (d) and (e) are similar to the two previous ones but for P3 and also with only one phase different from zero at a time. Instead, plot (f) shows the correlation in P2 and P3 between  $\sin \alpha_1$  and

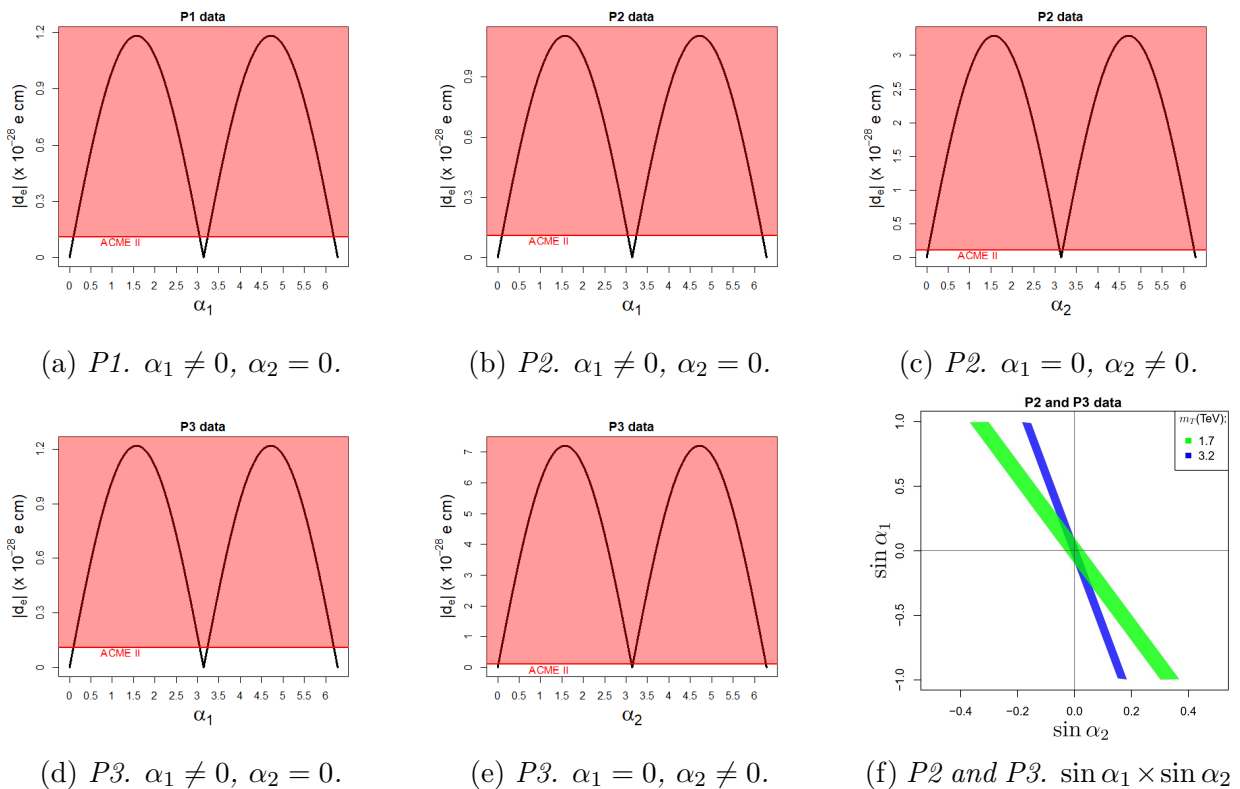


Figure 3: In plots (a)-(e), the electron EDM vs. one of the CPV phases. In white the allowed parameter space while in red the excluded region due to the ACME II bound in Eq. (1.1) by ACME II. In plot (f), the correlation between the two CPV phases, where the coloured regions represent the allowed parameter space, whose extremes saturate the ACME II bound. In green the *P2* benchmark and in blue the *P3* one.

$\sin \alpha_2$ .

Once only one phase is switched on at a time, the electron EDM constraint gives the following ranges for the phases:

$$\begin{aligned}
\text{Plot (a)} &\rightarrow \alpha_1 \in [-0.093, 0.093] \cup [\pi - 0.093, \pi + 0.093] \\
\text{Plot (b)} &\rightarrow \alpha_1 \in [-0.100, 0.100] \cup [\pi - 0.100, \pi + 0.100] \\
\text{Plot (c)} &\rightarrow \alpha_2 \in [-0.033, 0.033] \cup [\pi - 0.033, \pi + 0.033] \\
\text{Plot (d)} &\rightarrow \alpha_1 \in [-0.090, 0.090] \cup [\pi - 0.090, \pi + 0.090] \\
\text{Plot (e)} &\rightarrow \alpha_2 \in [-0.015, 0.015] \cup [\pi - 0.015, \pi + 0.015].
\end{aligned} \tag{3.9}$$

Notice that the constraints for  $\alpha_2$  are always stronger than those on  $\alpha_1$ : this is due to the fact that the effective scale suppressing  $y_1$  is one order of magnitude stronger than the one suppressing  $y_2$ , for both *P2* and *P3*.

It is interesting to compare these results with the constraints on the phases if EFT approach is used, with effective single mass scale. For instance, identifying the effective mass scale in  $d = 6$  operator used in Ref. [40] with the lightest state in the benchmark point *P1*,

one can see that in the  $ML\sigma M$  one order of magnitude larger phases are acceptable. This example illustrates the fact that effective scales used in the EFT approach overestimate the theoretically uncomfortable need for tuning in the phases.

Once both phases are non-vanishing, the parameter space opens even more up due to a partial cancellation present between the different contributions in Eq. (3.7). In particular, large values for the phases are allowed as far as the linear correlation is present between  $\sin \alpha_1$  and  $\sin \alpha_2$ . Furthermore, Fig. 3(f) shows the dependence on the scale of the top-partner mass: intuitively, the larger is this scale the smaller is the contributions to the EDM and the larger should be the allowed region for the phases. However, the plot shows the opposite behaviour. The reason is that the parameters controlling  $m_T$  are not the same as those entering  $\tilde{\kappa}_t$ : in particular, an explicit computation shows that the effective scale suppressing the EDM contribution associated to  $y_2$  is smaller for P3 than for P2 and consequently the allowed parameter space for  $\sin \alpha_2$  is smaller, although  $m_T$  is larger. To further investigate this aspect, Fig. 4 shows the largeness of the allowed interval for  $\sin \alpha_2$  for a fixed value of  $\sin \alpha_1$ : this is equivalent of measuring the vertical largeness of the bands in Fig. 3(f). Each point in Fig. 4 represent a different benchmark, where, however, the value of  $m_\sigma$  and of  $\sin^2 \gamma$  are the same as for the benchmarks P1, P2 and P3, while  $y_2 \in [3.0, 6.0]$  and  $y'_2 = 0$ . The plot shows that there is no correlation between the allowed values for  $\sin \alpha_2$  and  $m_T$ .

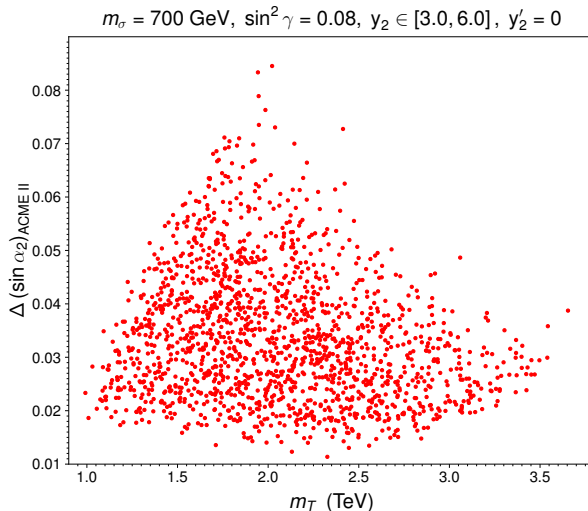


Figure 4: *Largeness of the allowed interval for  $\sin \alpha_2$  as a function of  $m_T$  for many different benchmark points, selecting  $m_\sigma = 700 \text{ GeV}$ ,  $\sin^2 \gamma = 0.08$ ,  $y_2 \in [3.0, 6.0]$  and  $y'_2 = 0$ .*

## 4 Electroweak Phase Transition

In Sect. 2.1 the range of parameters of the scalar sector that is consistent with the available data has been determined. Sect. 3 illustrated that the bounds on the pseudoscalar Yukawa couplings obtained from the electron EDM are consistent with the results

presented in the earlier literature. Those bounds are known to allow for successful electroweak baryogenesis, provided the electroweak phase transition is strong enough. At this point, there enters the structure of the ML $\sigma$ M model in two-fold way. First, after the bounds on  $\tilde{\kappa}_\psi$  being translated into the values of the model parameters, Sect. 3 showed the consistency with the precision electroweak data and briefly discussed the signatures of the new state production in colliders [38]. Secondly, given the parameters of the scalar sector, the character of the phase transition is in the ML $\sigma$ M uniquely determined and this is the subject of the present section: it is by far too weak to be consistent with the electroweak baryogenesis.

To analyze the phase transitions a model exhibits, the effective potential of the scalar sector at finite temperature needs to be studied. This is calculated using the methods presented in the Appendix A. At finite temperature, scalars receive thermal contribution to the mass, so above some critical temperature  $T_c$  the EW symmetry is restored.

EW baryogenesis requires a strong first order phase transition [41, 42, 44]. First order means that at the critical temperature, there must be a barrier in the effective potential between the two degenerate minima: the EW symmetric minimum at  $\mathbf{h} = 0$ , and the EW breaking minimum at  $\mathbf{h} = v_{\mathbf{h},c}$ . Then, the phase transition occurs through bubble nucleation: at  $T > T_c$  the plasma is in the EW symmetric phase, and at  $T < T_c$ , bubbles in the EW breaking phase will start to grow and percolate. This is a highly out-of-equilibrium process, and an excess of baryon number can be generated in the bubble walls [43, 45]. To explain the observed baryon number excess, the phase transition must also be strong enough:  $v_{\mathbf{h},c}/T_c > 0.6 - 1.6$  (see Refs. [56, 57]).

In the SM the phase transition has a cross over character (the Higgs gets a VEV smoothly without nucleation). It has been widely discussed in the literature that by adding a scalar to the potential one can obtain a first order phase transition, strong enough for a successful baryogenesis (see for instance Refs. [57–63]). In the ML $\sigma$ M there is an extra scalar  $\sigma$  which is the radial mode of a scalar 5-plet, whose VEV  $f$  breaks spontaneously the global  $SO(5)$  symmetry. However, as explained in detail below, several effects suppress its role in the phase transition. Those are: very strong experimental upper bound on the  $\mathbf{h} - \mathbf{s}$  mixing, the underlying  $SO(5)$  global symmetry of the potential and the hierarchy  $f/v_{\mathbf{h}} \gg 1$  at zero temperature.

## 4.1 Leading Temperature Corrections

The first step is to analyse the effective potential including only leading high temperature corrections (see Appendix A.1). This approximation can neglect important contributions from higher orders, but it gives a first analytic approach to the problem. In the next subsection the full numerical analysis will be performed. The effective potential in this approximation (A.14) has the same functional form as the tree level potential (2.2) with some temperature-dependent coefficients (up to constant terms):

$$V_{\text{eff},0}(\mathbf{h}, \mathbf{s}) = \lambda (\mathbf{h}^2 + \mathbf{s}^2 - f(T)^2)^2 + \alpha(T)f(T)^3\mathbf{s} - \beta(T)f(T)^2\mathbf{h}^2, \quad (4.1)$$

where

$$f(T)^2 = f^2 - \frac{7}{12}T^2, \quad (4.2)$$

$$\alpha(T) = \alpha \frac{f^3}{f(T)^3}, \quad (4.3)$$

$$\beta(T) = \frac{1}{f(T)^2} \left( f^2 \beta - \frac{T^2}{8v_{\mathbf{h}}^2} (m_Z^2 + 2m_W^2 + 2m_t^2) \right). \quad (4.4)$$

The possible first order phase transitions can be studied looking for the parameters that give a potential (4.1) with two degenerate minima. Then, evolving the parameters from  $T = T_c$  to  $T = 0$ , the zero temperature tree level parameters can be found [60]. However, if  $\alpha \neq 0$ , the potential (4.1) cannot even have two local minima if one of them breaks the EW symmetry. This potential has a stationary point with  $v_{\mathbf{h}} \neq 0$  if and only if the condition

$$f(T)^2 \alpha(T)^2 < 4 f(T)^2 \beta(T)^2 \left( 1 + \frac{\beta(T)}{2\lambda} \right) \quad (4.5)$$

is satisfied. Notice that, assuming  $f^2 > 0$ , this condition is the right inequality (2.6). The stationary point is unique (up to  $SO(4)$  transformations) and it is a minimum if and only if

$$f(T)^2 \beta(T) > 0. \quad (4.6)$$

If there is a second minimum, it has to be located along  $\mathbf{h} = 0$ . However, once the inequalities (4.5) and (4.6) are satisfied, all roots of  $\partial V_{\text{eff}}/\partial \mathbf{s}$  along  $\mathbf{h} = 0$  are contained in the interval where  $\partial^2 V_{\text{eff}}/\partial \mathbf{h}^2$  is negative. All stationary points along  $\mathbf{h} = 0$  are then either maxima or saddle points. Therefore, in this approximation all phase transitions are second order (VEVs evolve continuously with the temperature). The absence of a tree level barrier is related to the flat direction of the  $SO(5)$  potential, which is too weakly perturbed.<sup>1</sup>

The symmetry-breaking pattern as the temperature decreases is as follows. At very high temperatures, both  $f(T)^2$  and  $f(T)^2 \beta(T)$  are negative, so the masses for  $\mathbf{h}$  and  $\mathbf{s}$  at the origin are positive, and the  $SO(5)$  symmetry is not spontaneously broken. The  $f(T)^2$  is negative for temperatures higher than

$$T_{SO(5)} = \sqrt{\frac{12}{7}} f. \quad (4.7)$$

When the conditions (4.5) and (4.6) are satisfied, the EW symmetry is broken. The saturating point of (4.5) once  $f^2(T)\beta(T) \geq 0$  gives the EW critical temperature  $T_{EW}$ . If the zero-temperature parameters satisfy

$$\begin{aligned} \beta &< \frac{\alpha^{2/3} \lambda^{1/3}}{2^{1/3}} + \frac{3}{14v_{\mathbf{h}}^2} (m_Z^2 + 2m_W^2 + 2m_t^2) \\ &= \frac{\alpha^{2/3} \lambda^{1/3}}{2^{1/3}} + 0.287, \end{aligned} \quad (4.8)$$

---

<sup>1</sup>It remains to be seen if adding more  $SO(5)$ -breaking terms can give us a strong first order phase transition suitable for baryogenesis.

then  $T_{EW} < T_{SO(5)}$ . At  $T_{SO(5)}$ , the  $SO(5)$  symmetry is broken spontaneously but the EW symmetry is preserved because of the explicit  $SO(5)$  breaking. The VEV  $v_s(T)$  starts to receive increasing contributions from this breaking while  $v_h(T)$  keeps vanishing. The EW symmetry is later broken at a lower temperature. If the condition (4.8) is not satisfied, then  $T_{EW} \geq T_{SO(5)}$  and the EW symmetry is broken at the same time as the  $SO(5)$  symmetry, before  $f(T)^2$  becomes positive. However, in that case,  $f < v_h$  ( $T_{EW}$  is still at the EW scale), and it corresponds to a very tiny region in the allowed parameter space very close to the  $f^2 = 0$  limit.

## 4.2 Full Analysis

Although leading temperature contributions do not trigger a first order phase transition, it is well known that higher orders can generate a barrier from the bosonic contribution in the Higgs potential if the coupling between the Higgs and the scalar is large enough. A natural question is whether the loop-contribution of  $\mathbf{s}$  in the potential is enough to generate such a barrier in the EW phase transition.

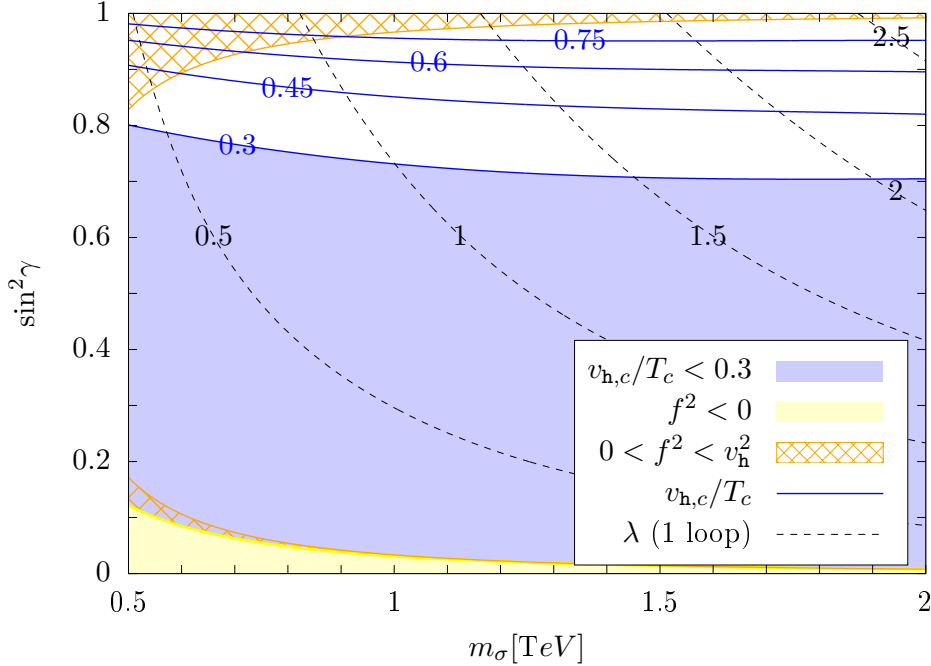


Figure 5: *Strength of the EW phase transition ( $v_{h,c}/T_c$ ) as function of the singlet mass ( $m_\sigma$ ) and the mixing angle ( $\sin^2 \gamma$ ). The blue solid lines correspond to  $v_{h,c}/T_c = 0.3, 0.45, 0.6, 0.75$ . In addition, the black dashed lines depict  $\lambda = 0.5, 1, 1.5, 2, 2.5$ , calculated with the one-loop effective potential. According to the criterion of Ref. [57], in the region where  $\lambda \gtrsim 1.5$ , the one-loop analysis of the phase transition breaks down due to higher loop corrections.*

If we assume  $v_h \ll f$  and  $T_{EW} \ll T_{SO(5)}$ , the VEV of  $\mathbf{s}$  will be approximately constant in the EW phase transition. If we perform a shift on  $\mathbf{s}$  to make  $v_s = 0$ , the situation

becomes similar to the one-step phase transition discussed in Ref. [57]. There, the EW phase transition for the SM plus a scalar that does not develop a VEV (before and after the phase transition) was studied. By analogy, in our case, the operator responsible for the barrier in the potential  $V(\mathbf{h}, v_s)$  is  $\mathbf{h}^2(\mathbf{s} - v_s)^2$ . In the ML $\sigma$ M, the coupling of this operator is  $2\lambda$ . Translating directly the results of Ref. [57] to the ML $\sigma$ M case one obtains that, if the mass of the singlet is in the range  $0.5 - 1$  TeV, the coupling must be  $\lambda \gtrsim 0.75 - 1.5$  for the phase transition to be relatively strong  $v_{h,c}/T_c \gtrsim 0.6$ . However, these values require a Higgs-singlet mixing  $\sin^2 \gamma > 0.7$  which is completely excluded (see Eq. (2.14)). This suggests that a strong first order phase transition is unlikely in the ML $\sigma$ M.

To confirm the previous argument, the full numerical calculation has been performed, including all finite temperature corrections up to one-loop and ring corrections according to Appendix A. The results are presented in Fig. 5. For the non-excluded low mixing angles ( $\sin^2 \gamma \lesssim 0.09$ ), the contribution of the singlet to the barrier is absolutely negligible. Because of this, the full range of the mixing angle is depicted in order to access to the range of parameters where the phase transition becomes strong. Indeed, only for completely excluded mixing angles  $\sin^2 \gamma \gtrsim 0.9$ , the system manifests a strong phase transition ( $v_{h,c}/T_c \gtrsim 0.6$ ).

## 5 Conclusions

We have reanalysed the bounds on the pseudoscalar Yukawa couplings of the third generation fermions following from the experimental upper limit on the electron EDM and confirm the recent results of Ref. [40]. As shown in that reference, those bounds are consistent with successful electroweak baryogenesis driven by a complex tau Yukawa coupling, provided the electroweak phase transition is strong enough.

We interpret the obtained strongest bound for the top Yukawa coupling in the framework on the Minimal Linear  $\sigma$  Model with complex couplings. This is an interesting, UV complete model, with the global  $SO(5)$  symmetry spontaneously broken by the radial mode of a scalar 5-plet and the Higgs field emerging as the Goldstone model. The  $SO(5)$  symmetry is explicitly broken by a minimal number of couplings needed for the self-consistency of the model. Due to the presence of the radial mode  $\sigma$  in the spectrum, the Yukawa couplings get BSM contributions which, in the low energy limit are obtained from  $d = 5$  operators with the Wilson coefficients calculated in terms of the original parameters of the model, couplings and mass parameters.

For several benchmark points of the Lagrangian parameters, consistent with other experimental constraints such as precision electroweak data and the upper limit on the Higgs and scalar singlet mixing, the bound on the top pseudoscalar Yukawa coupling is used to determine the acceptable range of new phases present in the model. We find that in the considered UV complete model, with several mass scales in the Lagrangian, the constraints on the values of the phases are significantly weaker than in the EFT approach with one effective mass scale identified with the lightest mass eigenstate of our model. Thus, the model provides an explicit example that the theoretically unnatural very strong suppression of new phases needed for consistency of the complex top Yukawa coupling with the EDM bound, which follows from the EFT approach with an effective NP mass scale

$\Lambda = \mathcal{O}(1 \text{ TeV})$ , need not to be the case in UV complete models with the lightest mass eigenstate in a similar range.

The UV complete model allows for an unambiguous calculation of the electroweak phase transition. In the allowed parameter range (Higgs and scalar singlet mixing), it turns out to be by far too weak for a successful baryogenesis. Thus, it explicitly illustrates the fact that the measurement of the CP violating Yukawa couplings is interesting in its own sake.

## Acknowledgements

We thank J. R. Espinosa, M. Olechowski, K. Sakurai, J. van de Vis and G. A. White for fruitful discussions. S.P. is grateful to Anna Lipniacka (Bergen University) for discussions on the prospects of measuring CPV in the tau Yukawa coupling.

J.A.G. and L.M. acknowledge partial financial support by the Spanish MINECO through the Centro de excelencia Severo Ochoa Program under grant SEV-2016-0597, by the Spanish ‘‘Agencia Estatal de Investigaci3n’’ (AEI) and the EU ‘‘Fondo Europeo de Desarrollo Regional’’ (FEDER) through the projects FPA2016-78645-P and PID2019-108892RB-I00/AEI/10.13039/501100011033. J.A.G. and L.M. also acknowledge support from the European Union’s Horizon 2020 research and innovation programme under the Marie Skłodowska-Curie grant agreement No 860881-HIDDeN. J.M.L. acknowledges financial support from the Polish National Science Center under the Beethoven series grant number DEC-2016/23/G/ST2/04301, and from the European Research Council (ERC) under the European Union’s Horizon 2020 research and innovation program under grant agreement 833280 (FLAY). L.M. acknowledges partial financial support by the Spanish MINECO through the ‘‘Ram3n y Cajal’’ programme (RYC-2015-17173). The research of S.P. has received funding from the Norwegian Financial Mechanism for years 2014-2021, grant nr 2019/34/H/ST2/00707.

## A Finite Temperature Effective Potential

In order to study possible phase transitions, we need to calculate the finite-temperature effective potential for the scalar sector. We will work at one loop including ring corrections:

$$V_{\text{eff}}(T; \phi) = V(\phi) + V_{\text{CW}}(\phi) + V_{\text{T}}(T; \phi) + V_{\text{r}}(T; \phi). \quad (\text{A.1})$$

Here,  $V$  is the tree level scalar potential (2.2),  $V_{\text{CW}}$  is the Coleman-Weinberg correction (one-loop zero temperature correction),  $V_{\text{T}}$  is the one-loop finite temperature correction, and  $V_{\text{r}}$ , the ring correction. It is convenient to keep all the components of the scalar  $\phi = (\pi_1, \pi_2, \pi_3, \mathbf{h}, \mathbf{s})$  because in the calculation of every piece of the effective potential we have to take into account the Goldstone bosons  $\vec{\pi}$ . Once computed, we can always take the unitary gauge  $\vec{\pi} = 0$ .

The Coleman-Weinberg correction [64] in  $\overline{\text{MS}}$  is given by

$$V_{\text{CW}}(\phi) = \sum_{i=(\phi, f, V)} (-1)^{F_i} \frac{n_i}{64\pi^2} \text{Tr} \left[ M_i^4 \left( \log \frac{M_i^2}{\mu_{\overline{\text{MS}}}^2} - C_i \right) \right]. \quad (\text{A.2})$$

Here,  $i$  runs over the different spin sectors  $i = (\phi, f, V)$  (scalars, fermions, and gauge bosons),  $F_i$  is the fermion number (1 for fermions, 0 for bosons), and  $M_i$  is the mass matrix for the sector  $i$  for a given vev for  $\phi = (\pi_1, \pi_2, \pi_3, \mathbf{h}, \mathbf{s})$ . For the scalar and vector sectors (in gauge basis):

$$(M_\phi^2)_{ab} = \frac{\partial^2 V}{\partial \phi^a \partial \phi^b}, \quad (\text{A.3})$$

$$M_V^2 = \frac{(\mathbf{h}^2 + \vec{\pi}^2)}{v_h^2} \begin{pmatrix} m_W^2 & 0 & 0 & 0 \\ 0 & m_W^2 & 0 & 0 \\ 0 & 0 & m_W^2 & -m_W \sqrt{m_Z^2 - m_W^2} \\ 0 & 0 & -m_W \sqrt{m_Z^2 - m_W^2} & m_Z^2 - m_W^2 \end{pmatrix}. \quad (\text{A.4})$$

In the fermion sector, we neglect the contributions from the effective operators of dimension 5 or higher of Tab. 3, and the contribution from all SM fermions except the top. The fermion sector reduces then to

$$M_f^2 = \frac{m_t^2}{v_h^2} (\mathbf{h}^2 + \vec{\pi}^2). \quad (\text{A.5})$$

Lastly,

$$n_i = (1, 12, 3), \quad (\text{A.6})$$

$$C_i = \left( \frac{3}{2}, \frac{3}{2}, \frac{5}{2} \right), \quad (\text{A.7})$$

where we have included the color factor in  $n_f$ . For the calculations in this work we set the renormalization scale to be  $\mu_{\overline{\text{MS}}} = v_h$ .

The one-loop finite temperature correction is [65, 66]

$$V_T(T; \phi) = \sum_{i=(\phi, f, V)} (-1)^{F_i} \frac{n_i T^4}{2\pi^2} \text{Tr} J_{F_i}(M_i^2/T^2), \quad (\text{A.8})$$

where  $J_0$  and  $J_1$  are the thermal bosonic and fermionic functions:

$$J_{F_i}(y^2) = \int_0^\infty dx x^2 \log \left[ 1 - (-1)^{F_i} e^{-\sqrt{x^2 + y^2}} \right]. \quad (\text{A.9})$$

Finally, if  $T \gg M_i$ , the so-called ring diagrams, which are bosonic multi-loop diagrams, can give important contributions due to large  $T/\mu_{\overline{\text{MS}}}$  ratios, so they have to be resummed [67]. For this we use the truncated full dressing method [68]:

$$V_r(T; \phi) = \sum_{i=(\phi, V)} \frac{T}{12\pi} \text{Tr} [M_i^3 - (M_i^2 + \Pi_i(T))^{3/2}], \quad (\text{A.10})$$

where  $\Pi_i$  is zero momentum thermal self-energies, that, in the high temperature limit are

$$(\Pi_\phi(T))_{ab} = \sum_{i=(\phi, f, V)} T^2 \frac{n'_i}{24} \frac{\partial^2 \text{Tr} M_i^2}{\partial \phi^a \partial \phi^b}, \quad (\text{A.11})$$

$$\Pi_V(T) = \frac{22}{3} \frac{T^2}{v_h^2} \text{diag}(m_W^2, m_W^2, m_W^2, m_Z^2 - m_W^2), \quad (\text{A.12})$$

where

$$n'_i = (1, 6, 3). \quad (\text{A.13})$$

Notice that both self-energies are  $\phi$ -independent: for the scalar self-energy, the squared mass matrix depends at most quadratically on the fields  $\phi^a$ .

## A.1 High Temperature Approximation

Expanding in the high temperature limit, the leading finite-temperature correction comes at order  $O(T^2)$  from the Taylor expansion of the thermal functions (A.9) around  $y^2 = 0$ . Including only these terms, the finite-temperature effective potential is

$$V_{\text{eff},0}(T; \phi) = V(\phi) + \sum_{i=(\phi,f,V)} T^2 \frac{n'_i}{24} \text{Tr} M_i^2. \quad (\text{A.14})$$

In this approximation, only the quadratic and linear terms of the potential receive finite temperature contributions.

## References

- [1] **Particle Data Group** Collaboration, P. Zyla *et. al.*, PTEP **2020** (2020), no. 8 083C01.
- [2] **ACME** Collaboration, V. Andreev *et. al.*, Nature **562** (2018), no. 7727 355–360.
- [3] M. Pospelov and A. Ritz, Annals Phys. **318** (2005) 119–169, [[hep-ph/0504231](#)].
- [4] V. Cirigliano and M. J. Ramsey-Musolf, Prog. Part. Nucl. Phys. **71** (2013) 2–20, [[arXiv:1304.0017](#)].
- [5] J. Engel, M. J. Ramsey-Musolf, and U. van Kolck, Prog. Part. Nucl. Phys. **71** (2013) 21–74, [[arXiv:1303.2371](#)].
- [6] F. Feruglio, B. Gavela, K. Kanshin, P. A. N. Machado, S. Rigolin, and S. Saa, JHEP **06** (2016) 038, [[arXiv:1603.05668](#)].
- [7] S. R. Coleman, J. Wess, and B. Zumino, Phys. Rev. **177** (1969) 2239–2247.
- [8] J. Callan, Curtis G., S. R. Coleman, J. Wess, and B. Zumino, Phys. Rev. **177** (1969) 2247–2250.
- [9] D. B. Kaplan and H. Georgi, Phys. Lett. **B136** (1984) 183–186.
- [10] D. B. Kaplan, H. Georgi, and S. Dimopoulos, Phys. Lett. **B136** (1984) 187–190.
- [11] T. Banks, Nucl. Phys. **B243** (1984) 125–130.
- [12] M. J. Dugan, H. Georgi, and D. B. Kaplan, Nucl. Phys. **B254** (1985) 299–326.
- [13] K. Agashe, R. Contino, and A. Pomarol, Nucl. Phys. **B719** (2005) 165–187, [[hep-ph/0412089](#)].
- [14] R. Barbieri, B. Bellazzini, V. S. Rychkov, and A. Varagnolo, Phys. Rev. **D76** (2007) 115008, [[arXiv:0706.0432](#)].
- [15] B. Gripaios, A. Pomarol, F. Riva, and J. Serra, JHEP **04** (2009) 070, [[arXiv:0902.1483](#)].
- [16] R. Alonso, I. Brivio, B. Gavela, L. Merlo, and S. Rigolin, JHEP **12** (2014) 034, [[arXiv:1409.1589](#)].
- [17] I. M. Hierro, L. Merlo, and S. Rigolin, JHEP **04** (2016) 016, [[arXiv:1510.07899](#)].
- [18] D. B. Kaplan, Nucl. Phys. **B365** (1991) 259–278.
- [19] R. Contino and A. Pomarol, JHEP **11** (2004) 058, [[hep-th/0406257](#)].

- [20] M. B. Gavela, K. Kanshin, P. A. N. Machado, and S. Saa, *Eur. Phys. J.* **C76** (2016), no. 12 690, [[arXiv:1610.08083](#)].
- [21] F. Feruglio, *Int. J. Mod. Phys.* **A8** (1993) 4937–4972, [[hep-ph/9301281](#)].
- [22] R. Contino, C. Grojean, M. Moretti, F. Piccinini, and R. Rattazzi, *JHEP* **05** (2010) 089, [[arXiv:1002.1011](#)].
- [23] R. Alonso, M. B. Gavela, L. Merlo, S. Rigolin, and J. Yepes, *Phys. Lett.* **B722** (2013) 330–335, [[arXiv:1212.3305](#)]. [Erratum: *Phys. Lett.*B726,926(2013)].
- [24] R. Alonso, M. B. Gavela, L. Merlo, S. Rigolin, and J. Yepes, *Phys. Rev.* **D87** (2013), no. 5 055019, [[arXiv:1212.3307](#)].
- [25] G. Buchalla, O. Catà, and C. Krause, *Nucl. Phys.* **B880** (2014) 552–573, [[arXiv:1307.5017](#)]. [Erratum: *Nucl. Phys.*B913,475(2016)].
- [26] I. Brivio, T. Corbett, O. J. P. Éboli, M. B. Gavela, J. Gonzalez-Fraile, M. C. Gonzalez-Garcia, L. Merlo, and S. Rigolin, *JHEP* **03** (2014) 024, [[arXiv:1311.1823](#)].
- [27] I. Brivio, O. J. P. Éboli, M. B. Gavela, M. C. Gonzalez-Garcia, L. Merlo, and S. Rigolin, *JHEP* **12** (2014) 004, [[arXiv:1405.5412](#)].
- [28] M. B. Gavela, J. Gonzalez-Fraile, M. C. Gonzalez-Garcia, L. Merlo, S. Rigolin, and J. Yepes, *JHEP* **10** (2014) 044, [[arXiv:1406.6367](#)].
- [29] M. B. Gavela, K. Kanshin, P. A. N. Machado, and S. Saa, *JHEP* **03** (2015) 043, [[arXiv:1409.1571](#)].
- [30] O. J. P. Éboli and M. C. Gonzalez-Garcia, *Phys. Rev.* **D93** (2016), no. 9 093013, [[arXiv:1604.03555](#)].
- [31] I. Brivio, J. Gonzalez-Fraile, M. C. Gonzalez-Garcia, and L. Merlo, *Eur. Phys. J.* **C76** (2016), no. 7 416, [[arXiv:1604.06801](#)].
- [32] L. Merlo, S. Saa, and M. Sacristán-Barbero, *Eur. Phys. J.* **C77** (2017), no. 3 185, [[arXiv:1612.04832](#)].
- [33] R. Alonso, K. Kanshin, and S. Saa, *Phys. Rev.* **D97** (2018), no. 3 035010, [[arXiv:1710.06848](#)].
- [34] P. Kozów, L. Merlo, S. Pokorski, and M. Szleper, *JHEP* **07** (2019) 021, [[arXiv:1905.03354](#)].
- [35] I. Brivio, M. B. Gavela, S. Pascoli, R. del Rey, and S. Saa, *Chin. J. Phys.* **61** (2019) 55–71, [[arXiv:1710.07715](#)].
- [36] L. Merlo, F. Pobbe, and S. Rigolin, *Eur. Phys. J.* **C78** (2018), no. 5 415, [[arXiv:1710.10500](#)].
- [37] J. Alonso-González, L. Merlo, F. Pobbe, S. Rigolin, and O. Sumensari, *Nucl. Phys.* **B950** (2020) 114839, [[arXiv:1807.08643](#)].
- [38] J. Aguilar-Saavedra, J. Alonso-González, L. Merlo, and J. No, *Phys. Rev. D* **101** (2020), no. 3 035015, [[arXiv:1911.10202](#)].
- [39] J. Brod, U. Haisch, and J. Zupan, *JHEP* **11** (2013) 180, [[arXiv:1310.1385](#)].
- [40] E. Fuchs, M. Losada, Y. Nir, and Y. Viernik, *JHEP* **05** (2020) 056, [[arXiv:2003.00099](#)].
- [41] A. Sakharov, *Sov. Phys. Usp.* **34** (1991), no. 5 392–393.
- [42] V. Kuzmin, V. Rubakov, and M. Shaposhnikov, *Phys. Lett. B* **155** (1985) 36.
- [43] A. G. Cohen, D. Kaplan, and A. Nelson, *Ann. Rev. Nucl. Part. Sci.* **43** (1993) 27–70, [[hep-ph/9302210](#)].
- [44] A. Riotto and M. Trodden, *Ann. Rev. Nucl. Part. Sci.* **49** (1999) 35–75, [[hep-ph/9901362](#)].
- [45] D. E. Morrissey and M. J. Ramsey-Musolf, *New J. Phys.* **14** (2012) 125003, [[arXiv:1206.2942](#)].

- [46] **ATLAS** Collaboration, G. Aad *et. al.*, Phys. Rev. **D101** (2020) 012002, [[arXiv:1909.02845](#)].
- [47] **ATLAS** Collaboration, M. Aaboud *et. al.*, Phys. Rev. **D98** (2018), no. 5 052008, [[arXiv:1808.02380](#)].
- [48] G. D’Ambrosio, G. F. Giudice, G. Isidori, and A. Strumia, Nucl. Phys. **B645** (2002) 155–187, [[hep-ph/0207036](#)].
- [49] V. Cirigliano, B. Grinstein, G. Isidori, and M. B. Wise, Nucl. Phys. **B728** (2005) 121–134, [[hep-ph/0507001](#)].
- [50] S. Davidson and F. Palorini, Phys. Lett. **B642** (2006) 72–80, [[hep-ph/0607329](#)].
- [51] R. Alonso, G. Isidori, L. Merlo, L. A. Munoz, and E. Nardi, JHEP **06** (2011) 037, [[arXiv:1103.5461](#)].
- [52] D. N. Dinh, L. Merlo, S. T. Petcov, and R. Vega-Álvarez, JHEP **07** (2017) 089, [[arXiv:1705.09284](#)].
- [53] B. Grzadkowski, M. Iskrzynski, M. Misiak, and J. Rosiek, JHEP **10** (2010) 085, [[arXiv:1008.4884](#)].
- [54] G. Lepage, preprint CLNS-80/447 (March, 1980).
- [55] T. Hahn, Computer Physics Communications **168** (Jun, 2005) 78–95.
- [56] H. H. Patel and M. J. Ramsey-Musolf, JHEP **07** (2011) 029, [[arXiv:1101.4665](#)].
- [57] D. Curtin, P. Meade, and C.-T. Yu, JHEP **11** (2014) 127, [[arXiv:1409.0005](#)].
- [58] S. Profumo, M. J. Ramsey-Musolf, and G. Shaughnessy, JHEP **08** (2007) 010, [[arXiv:0705.2425](#)].
- [59] A. Ashoorioon and T. Konstandin, JHEP **07** (2009) 086, [[arXiv:0904.0353](#)].
- [60] J. R. Espinosa, T. Konstandin, and F. Riva, Nucl. Phys. B **854** (2012) 592–630, [[arXiv:1107.5441](#)].
- [61] J. M. Cline, K. Kainulainen, P. Scott, and C. Weniger, Phys. Rev. D **88** (2013) 055025, [[arXiv:1306.4710](#)]. [Erratum: Phys.Rev.D 92, 039906 (2015)].
- [62] T. Alanne, K. Tuominen, and V. Vaskonen, Nucl. Phys. B **889** (2014) 692–711, [[arXiv:1407.0688](#)].
- [63] S. Profumo, M. J. Ramsey-Musolf, C. L. Wainwright, and P. Winslow, Phys. Rev. D **91** (2015), no. 3 035018, [[arXiv:1407.5342](#)].
- [64] S. R. Coleman and E. J. Weinberg, Phys. Rev. D **7** (1973) 1888–1910.
- [65] L. Dolan and R. Jackiw, Phys. Rev. D **9** (1974) 3320–3341.
- [66] S. Weinberg, Phys. Rev. D **9** (1974) 3357–3378.
- [67] C. Delaunay, C. Grojean, and J. D. Wells, JHEP **04** (2008) 029, [[arXiv:0711.2511](#)].
- [68] D. Curtin, P. Meade, and H. Ramani, Eur. Phys. J. C **78** (2018), no. 9 787, [[arXiv:1612.00466](#)].